

PURIFICATION OF THE ALPHA SUBUNIT OF THE EPITHELIAL SODIUM CHANNEL (α ENAC)
FOR SURFACE PLASMON RESONANCE (SPR) STUDIES

by

Chance N. Berman, B.S

A thesis submitted to the Graduate Council of
Texas State University in partial fulfillment
of the requirements for the degree of
Master of Science
with a Major in Biochemistry
December 2016

Committee Members:

Rachell Booth, Chair

Wendi David

Karen Lewis

COPYRIGHT

by

Chance Novelli Berman

2016

FAIR USE AND AUTHOR'S PERMISSION STATEMENT

Fair Use

This work is protected by the Copyright Laws of the United States (Public Law 94-553, section 107). Consistent with fair use as defined in the Copyright Laws, brief quotations from this material are allowed with proper acknowledgment. Use of this material for financial gain without the author's express written permission is not allowed.

Duplication Permission

As the copyright holder of this work I, Chance Novelli Berman, authorize duplication of this work, in whole or in part, for educational or scholarly purposes only with written permission.

ACKNOWLEDGEMENTS

I would first like to thank Dr. Rachell Booth for all her guidance and support with this project. I joined Dr. Booth's lab during my undergraduate junior year with course lab experience only. She welcomed me in the lab and gave me the opportunity to conduct scientific research. Without her extreme patients and support throughout my undergraduate career and graduate career, she allowed me to explore the world of scientific research which in turn helped me flourish as a graduate student. In addition to Dr. Booth, I would like to thank my committee members, Dr. Wendi David and Dr. Karen Lewis, whose guidance and support for my research was paramount to my success in graduate school.

Secondly, I would like to thank all the members of the Booth research lab, past and present, who have aided me along the way especially Samantha Swann who introduced me to Dr. Booth when I was an undergraduate teachers assistant. Without her I would never have indulged into scientific research and most likely would not have pursued my graduate degree. Also, to all the other lab members I got the privilege to work with over the last 3 years which added to my success and their assistance should not go unnoticed.

Lastly I would like to thank my family. My parents, Jerry and Marina, who were always guiding and supporting me to always strive to do better throughout my college career. I would also like to thank my best friend, my wife, Skyler Berman. Her unconditional love, patients, and support throughout this journey drove me to become the man I am today.

TABLE OF CONTENTS

	Page
ACKNOWLEDGEMENTS.....	iv
LIST OF TABLES.....	vii
LIST OF FIGURES.....	viii
ABSTRACT.....	xi
CHAPTER	
I. INTRODUCTION AND LITERATURE REVIEW	1
II. MATERIALS AND METHODS.....	13
III. RESULTS AND DISCUSSION	27
IV. CONCLUSION.....	70
LITERATURE CITED	73

LIST OF TABLES

Table	Page
1. PCR primers used	14
2. Peptide sequences	21
3. Concentrations of peptide/protein injections and interactions with immobilized peptide	26
4. ENaC peptides and their location	43
5. Summary of ENaC peptide Fractions quantitated	54
6. GST-E438 vs N285 kinetics	58
7. GST-N285 vs E438 kinetics	59
8. GST-E254 vs Q444 kinetics	60
9. GST-Q444 vs E254 kinetics	62
10. GST-E438 vs α ENaC kinetics	63
11. GST-N285 vs α ENaC kinetics	64
12. GST-E254 vs α ENaC kinetics	65
13. GST-E438 vs α His2- α ENaC kinetics	67
14. GST-N285 vs α His2- α ENaC kinetics	68
15. GST-E254 vs α His2- α ENaC kinetics	69
16. Summary of Kinetics	72

LIST OF FIGURES

Figure	Page
1. Cross-sectional area of the kidney with emphasis on the nephron	2
2. Depiction of epithelial cells which line the distal convoluted tubules, representing the movement of sodium and potassium ions through the cell.....	3
3. ENaC/DEG family conserved protein sequences	4
4. Predicted heterotrimeric structure of ENaC.....	5
5. Predicted quaternary and secondary structure of ENaC.....	6
6. Regulation of ENaC in an epithelial cell	9
7. Polymerase Chain Reaction (PCR) of α His2- α ENaC gene from pm α His2- α ENaC plasmid DNA	28
8. Gel extraction of digested α His2- α ENaC PCR product and digested pYES2/NTA plasmid DNA.....	29
9. pYES2/NTA/ α His2- α ENaC plasmid isolation and digestion from Top 10™ <i>E. coli</i> cells to verify cloning	32
10. Survival dilution growth “pronging” assay in BY4742 yeast cells.....	33
11. Survival dilution growth “pronging” assay in S1 yeast cells	34
12. Western blot analysis of α His2- α ENaC using different lysis conditions.....	36
13. Western blot analysis of α His2- α ENaC time course in BY4742 yeast strain	39
14. Western blot analysis of α His2- α ENaC time course in S1 yeast strain.....	40

15. IMAC purification of α His2- α ENaC analyzed by western blotting.....	42
16. Plasmid Isolation of ENaC ligand genes	43
17. Expressed GST-ENaC fusion proteins in total cell lysate	46
18. ISAC purification of GST-N285 analyzed by SDS-PAGE	50
19. ISAC purification of GST-E254 analyzed by SDS-PAGE.....	51
20. ISAC purification of GST-E438 analyzed by SDS-PAGE.....	52
21. ISAC purification of GST-Q444 analyzed by SDS-PAGE	53
22. CM5 chip activation and immobilization of GST-E438	56
23. Kinetic evaluation of binding assay of N285 analyte to GST fusion peptide E438	57
24. Kinetic evaluation of binding assay of E438 analyte to GST fusion peptide N285	59
25. Kinetic evaluation of binding assay of Q444 analyte to GST fusion peptide E254	60
26. Kinetic evaluation of binding assay of E254 analyte to GST fusion peptide Q444	61
27. Kinetic evaluation of binding assay of α ENaC analyte to GST fusion peptide E438	63
28. Kinetic evaluation of binding assay of α ENaC analyte to GST fusion peptide N285	64
29. Kinetic evaluation of binding assay of α ENaC analyte to GST fusion peptide E254	65
30. Kinetic evaluation of binding assay of α His2- α ENaC analyte to GST fusion peptide E438	66

31. Kinetic evaluation of binding assay of α His2- α ENaC analyte to GST fusion peptide N285	68
32. Kinetic evaluation of binding assay of α His2- α ENaC analyte to GST fusion peptide E254	69

ABSTRACT

The epithelial sodium channel (ENaC) is responsible for sodium reabsorption in the distal convoluted tubules of the nephron in the kidneys. ENaC is a transmembrane protein with N and C-termini located in the cytosol and a larger extracellular loop containing a wrist, palm, beta-ball, thumb, knuckle and finger. Due to ENaCs hydrophilic and hydrophobic nature, isolation and purification while still being functional is not well understood. A 6x histidine tag was engineered into the extracellular loop of α ENaC, referred to hereon as α His2- α ENaC, and then was subcloned in the yeast expression vector pYES2/NTA. pYES2/NTA/ α His2- α ENaC was transformed into S1, MAT α ura3-52 leu2-3,112 trp1-289 his7-2 ade5-1 lys2::InsE-4A, and BY4742, MAT α his3 Δ 1 leu2 Δ lys2 Δ ura3 Δ ygr204::kanMX4, yeast strains. Serial dilution assays, time-course expression trials, immobilized metal affinity chromatography (IMAC) and western blot analysis were employed to purify and verify expression of α His2 in each strain of *Saccharomyces cerevisiae*. ENaC peptides of each subunit were previously engineered and subcloned in the bacterial expression vector pGEX-4T-2. Immobilized substrate affinity chromatography (ISAC) was employed to purify peptides. Surface Plasmon Resonance (SPR) was conducted between ENaC peptides and whole subunit α His2- α ENaC. We report that the interactions of the palm and thumb region of β ENaC, independently, between the whole α ENaC subunit gave kinetic constants in the non-covalent range,

potentially being an inter-subunit binding domain. Additional studies would use longer peptides, thought to be portions/ whole binding domains, to further elucidate inter-subunit binding regions.

I. INTRODUCTION AND LITERATURE REVIEW

The ability of the human body to osmotically regulate sodium is critical for the circulatory system to maintain a physiological blood pressure. Deviations from homeostasis cause diseases such as heart, renal, hypertension, and hypotension (1). Regulation of sodium occurs in epithelial cells in the pulmonary system, colorectal system, and distal tubules of the kidney. Fine-tuning of sodium reabsorption is, in part, accomplished in these organs by the up or down regulation of the epithelial sodium channel, ENaC (2).

The kidney is composed of millions of functional units called nephrons (FIG 1). Nephrons regulate the concentration of water and solutes by filtering the blood and excreting the filtrate as urine. This is accomplished by blood being pumped to the glomerulus via an afferent arteriole, where capillaries aid in filtering solutes in the blood by size. Ions such as sodium and molecules such as glucose pass through the Bowman's capsule while proteins that do not meet the molecular weight cut off are expelled, with filtered blood, via an efferent arteriole. The filtrate is excreted into the Bowman's capsule through the proximal convoluted tubules, where pH is regulated by exchanging hydronium ions in the intersitium with bicarbonate ions from the filtrate. The proximal convoluted tubule is responsible for the majority of sodium reabsorption. The filtrate passes down the Loop of Henle, where water is removed via aquaporins and a urea concentration gradient is established from the filtrate. The filtrate ascends up to the

distal convoluted tubule where ENaC is located, and then moves to the collecting ducts where it is expelled as urine.

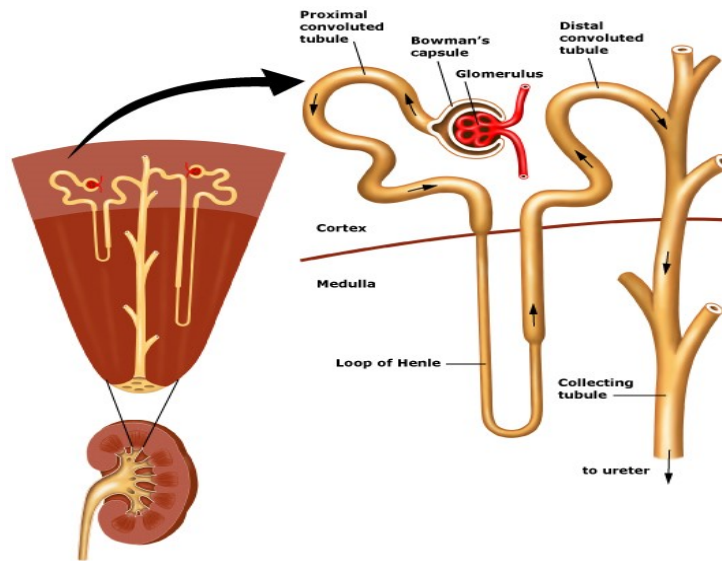


FIG 1. Cross-sectional area of the kidney with emphasis on the nephron. Filtration of our blood occurs in the kidneys where sodium ion reabsorption by ENaC transpires in the distal convoluted tubule of the nephron. Figure adapted from (3).

ENaC is located on the apical side of epithelial cells, and is responsible for reabsorbing sodium from the urine. It is classified as a non-voltage, constitutively open, amiloride-sensitive channel (FIG 2). ENaC works in conjunction with the sodium potassium pump on the basolateral side of the epithelial cell to maintain homeostasis in the cell (4). Variations in expression levels cause a divergence from homeostasis as ENaC is responsible for the last 2 – 5 % of sodium reabsorption (5).

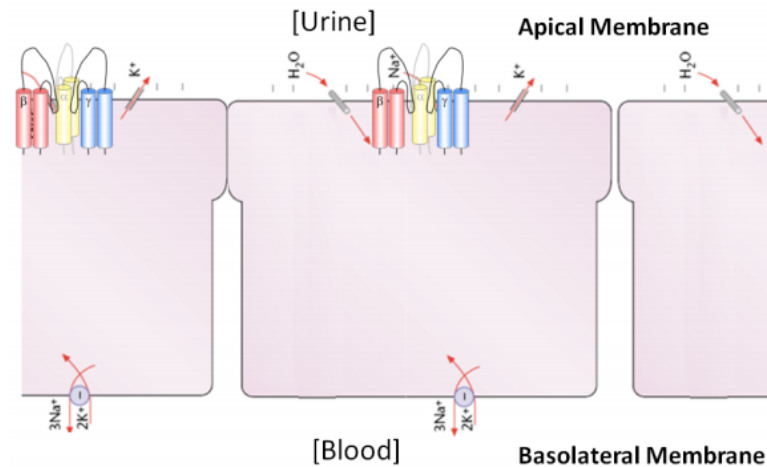


FIG 2. Depiction of epithelial cells which line the distal convoluted tubules, representing the movement of sodium and potassium ions through the cell. Sodium ions enter epithelial cells through ENaC located on the apical membrane of epithelial cells. To maintain osmotic pressure, water is drawn in and out of epithelial cells through aquaporins. Sodium ions are able to enter the bloodstream through the Na^+/K^+ -ATPase channel, facilitating the transfer of potassium into epithelial cells to be later excreted as urine. Figure adapted from (6).

ENaC belongs to the ENaC/Degenerin superfamily of cation channels.

Superfamilies' are characterized by their similarity in conserved structural features.

Conserved structural features in the cation channel family include cysteine rich domains (CRD), two membrane spanning domains (M1, M2), the extracellular loop, N and C-terminal cytosolic ends (FIG 3 A & B). Along with ENaC, the acid sensing ion channel (ASIC) and the ripped pocket/ pickedpocket (rpk/ppk) share similar structural features.

The acid sensing ion channel functions in sensory neurons via pumping protons, creating an acidic environment. The rpk/ppk has been seen to function in *Drosophila* larva through transduction of mechanical stimuli from heat. ENaC/Degenerin has been seen to function in *C. elegans* through transduction of mechanical stimuli via sodium reabsorption (7).

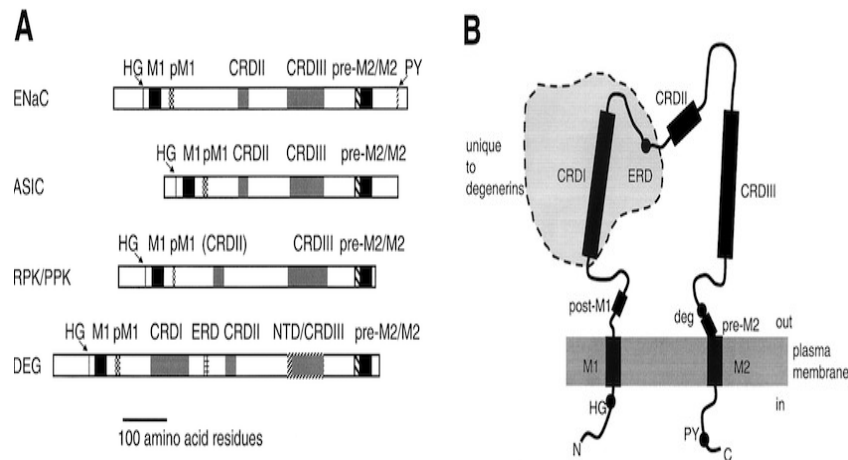


FIG 3. ENaC/DEG family conserved protein sequences. (A) Conserved domains between ENaC/DEG members. (B) Structure of an individual ENaC/DEG subunit where CRDI and ERD are specifically unique to the superfamily. Figure adapted from (8).

An ENaC structural model was developed based on ASIC1 crystal structure (FIG 4). Renal ENaC is composed of three subunits, α , β , γ , however there is a δ subunit, synonymous to the α subunit, present in pulmonary and colorectal organs (9). Each subunit is encoded by a separate gene, SCNN1A, SCNN1B, and SCNN1G, respectively. ENaC subunit stoichiometry is thought to be a 1:1:1 subunit ratio based on the highly conserved homology with ASIC1 (10). Speculation of the stoichiometry arises due to ENaC's low expression levels and obtaining high enough concentrations to form crystals. α ENaC can form a functional homotrimeric channel, although the homotrimeric showed lower sodium reabsorption compared to the heterotrimeric complex, $\alpha\beta\gamma$, in electrophysiological studies (11). The β and γ subunits cannot form a functional channel without the presence of the α subunit (12). Due to α ENaC's ability to form functional homotrimeric channels, it has been speculated that the α subunit could possibly form an

inner channel ring where the β and γ subunits interact with posterior regions of the α subunit channel ring (13).

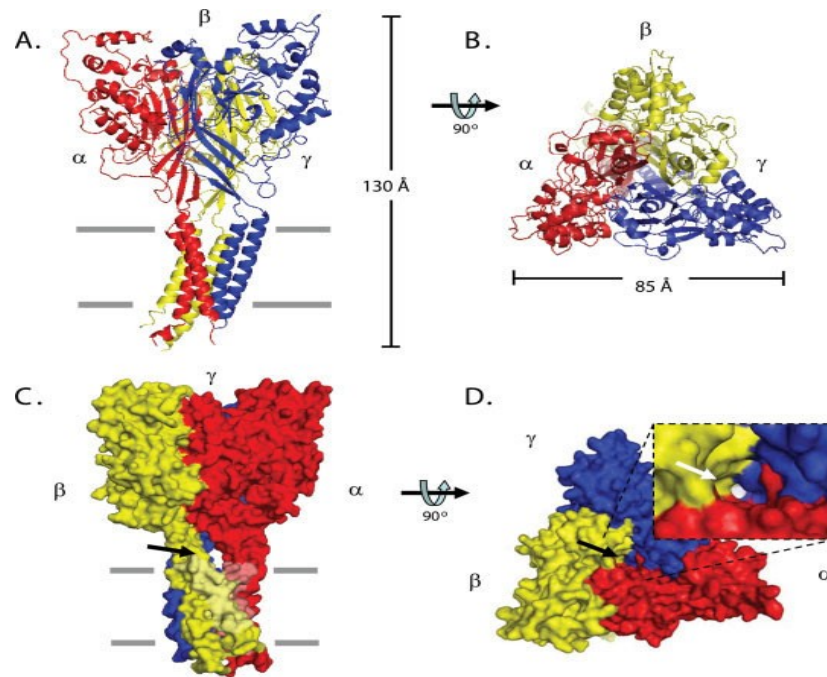


FIG 4. Predicted heterotrimeric structure of ENaC. (A & B) Ribbon diagrams for the predicted structure of ENaC showing the (A) lateral view and an (B) orthogonal aerial view. (C and D) Space filling models of ENaC from the (C) lateral view and an (D) orthogonal aerial view. Black arrows indicate expected pore location adapted from (14).

Previous studies have potentially identified regions between ENaC subunits with increased electron density based on X-ray crystallography of cASIC (15). Short peptides of each ENaC subunit were chosen based on charged residues in the electron dense regions through to participate in electrostatic interactions. ENaC peptide N285 is a portion of the α subunit located in the palm region which is composed of antiparallel β -sheets, facing the inner core (FIG 5). ENaC peptide E438 is a portion of the β subunit located in the thumb region which is composed of two α -helices, facing the extracellular

space (FIG 5). ENaC peptide E254 is a portion of the β subunit located in the palm region of the β subunit with a similar composition as that of N285 (FIG 5). ENaC peptide Q444 is a portion of the γ subunit located in the thumb region with a similar composition as that of E438 (FIG 5).

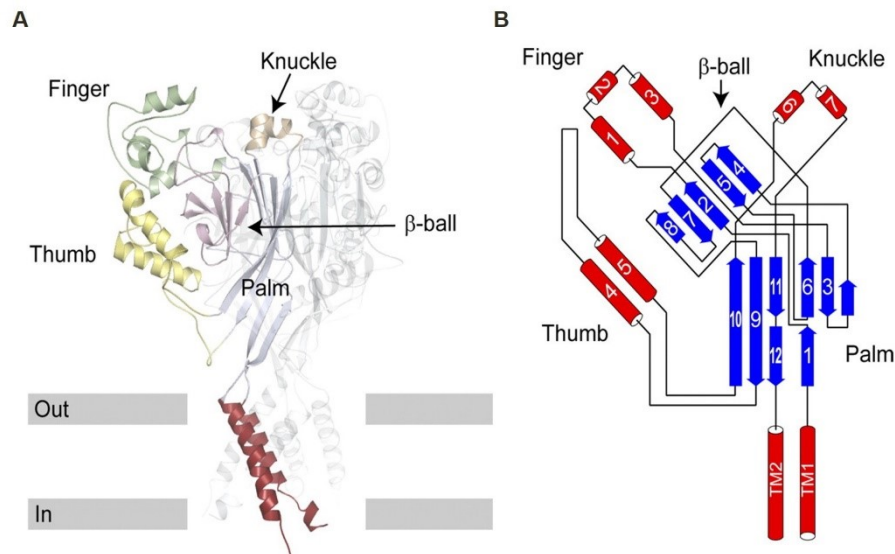


FIG 5. Predicted quaternary and secondary structure of ENaC. (A & B) “Hand” diagram predicted structure of ENaC showing the (A) quaternary structure and a (B) two-dimensional layout of an ENaC subunit. Figure adapted from (16).

Trafficking ENaC to the apical surface has been linked to several pathways and proteins known for epithelial cells. Maturation of ENaC involves processing through the endoplasmic reticulum (ER) followed by the Golgi apparatus via an Asn-linked glycan, to the apical surface. There is evidence that a subset of ENaC bypasses the Golgi complex via premature *N*-linked glycans (17). These channels have been seen in the apical membrane surface without glycan signaling. There has also been evidence for ENaC

trafficking via both a lipid raft-association and raft-free regulation (17). Studies for targeting ENaC from the trans golgi network (TGN) have shown ENaC-coated vesicles utilize the cytoskeleton and molecular motors to shuttle ENaC to the apical membrane. This was demonstrated by interrupting actin or tubulin causing a loss of ENaC transport to the apical membrane (17). Disruption of soluble N-ethylmaleimide-sensitive factor attachment protein receptor (SNARE), responsible for final vesical fusion to the membrane, and SNARE binding proteins prevented exocytosis of ENaC vesicles with apical membrane (18).

ENaC placement in the apical membrane is regulated by vasopressin, an antidiuretic hormone (ADH), aldosterone, a mineralocorticoid hormone, and Nedd4, a ubiquitin ligase (FIG 6). ENaC is up-regulated by vasopressin and aldosterone.

Vasopressin regulates the water retention by increasing water reabsorption in the kidney's collecting ducts namely the nephron by aquaporins and it also functions to constrict blood vessels. Vasopressin is produced in the hypothalamus and stored at the posterior pituitary to later be released into the bloodstream. Vasopressin binds to cell surface receptors on the basolateral membrane which triggers a cAMP signaling pathway (FIG 6). Increased cellular levels of cAMP activates Protein Kinase A (PKA) to assist SNAREs for exocytosis of ENaC-containing vesicles to the apical membrane (FIG 6). Vasopressin also up regulates aquaporin-2 trafficking to the apical membrane to maintain osmotic pressure and homeostasis of epithelial cells (19).

Aldosterone regulates plasma sodium, extracellular potassium and arterial blood pressure. It accomplishes this by acting directly on the distal tubules and collecting ducts of the nephron. Aldosterone is produced in the zona glomerulosa of the adrenal cortex in the adrenal gland and is then activated by renin, an enzyme produced in the juxtaglomerular cells. It is activated by cleaving angiotensinogen, a peptide hormone responsible for vasoconstriction produced by the liver, to form angiotensin I. This intermediate product is further converted to angiotensin II by angiotensin-converting enzyme (ACE), located in the pulmonary capillaries. Angiotensin II constricts the blood vessels which in turn increases secretion of vasopressin and aldosterone therefore stimulating the hypothalamus to activate. Aldosterone binds to cell surface receptors on the basolateral membrane in which it is then transported to the nucleus where it promotes transcription of ENaC mRNA (FIG 6). Aldosterone additionally promotes the up-regulation in the transcription of serum and glucocorticoid-regulated kinase 1 (SGK1) further upregulating ENaC (20).

When ENaC is being down regulated the HECT domain of Nedd4-2, located on the C-terminal, is ubiquitinated followed by poly-ubiquitination resulting in endocytosis of ENaC and is transported for lysosomal degradation (21, 22). ENaC is up-regulated by SGK1, phosphorylating the WW domain of Nedd4-2, an E3 ubiquitin ligase responsible for down regulation, blocking the interaction of the WW domain of Nedd4-2 with the C-terminal PY motif of ENaC (FIG 6). Studies have shown that the protein 14-3-3 isoform 14-3-3 β is induced by aldosterone, interacting with the phosphorylated WW domain

and further interrupting the interaction between the PY motif on ENaC and the WW domain (23, 24).

Sodium reabsorption is directly proportional on the amount of functional ENaC channels present in the apical membrane at one time (25). Regulation of ENaC and cellular elements effect the lifecycle and the quantity of channels trafficked to the apical membrane. Consequently, modifications to ENaC can lead to a rise of varying associated diseases.

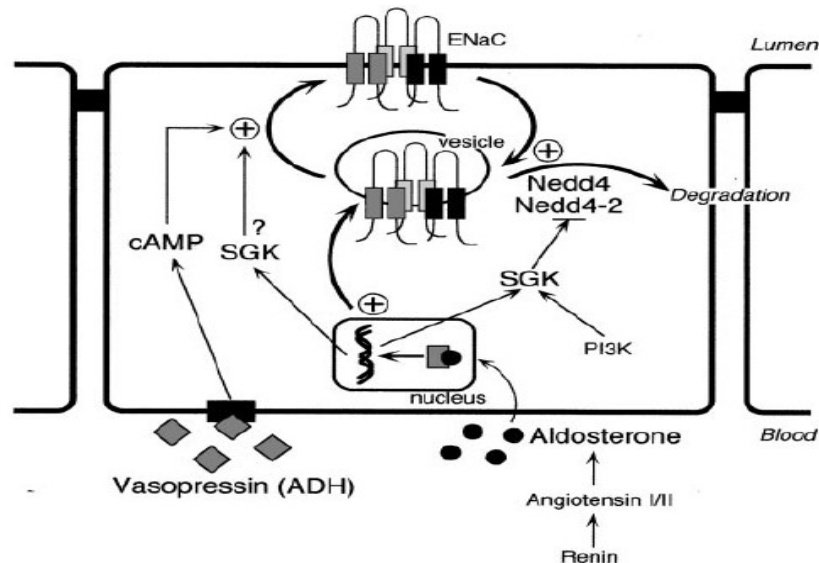


FIG 6. Regulation of ENaC in an epithelial cell. Hormones, vasopressin and aldosterone, promote up-regulation of ENaC for apical membrane insertion. Nedd4-2 is responsible for tagging ENaC for ubiquitination. Figure adapted from (26).

Mis-regulation and mutations of heterotrimeric ENaC give rise to physiological diseases in humans include Liddle's Syndrome and Pseudohypoaldosteronism Type 1 (PHA-1) (27, 28). In addition, mutations in ENaC have also been associated with Crohn's Disease and cystic fibrosis (29, 30).

Liddle's Syndrome (pseudohyperaldosteronism) is an autosomal dominant gain-of-function disease that causes an excess of reabsorption of sodium ions and decrease of potassium ions into the circulatory system therefore giving rise to hypertension and hypokalemia. Additional effects include low plasma renin activity and metabolic alkalosis. This is due to a deletion of 45 to 75 amino acids from the C-terminus of the β and γ subunit of ENaC. This deletion removes the PY motif which hinders the ability of Nedd4-2 to regulate the degradation of ENaC (31). Children are frequently asymptomatic, whereas adults exhibit weakness, fatigue, cardiac arrhythmia, and myasthenia (31).

PHA-1 is a loss-of-function disease categorized in two separate classes: renal PHA-1, an autosomal dominant disease, and systemic PHA-1, an autosomal recessive disease. Both types are generalized by salt wasting, high concentration of salts in the urine, leading to hypotension and hyperkalemia. While both have effects on the kidneys, systemic affects eccrine glands, salivary glands, and the colorectal organ (32). This arises from either C133Y mutation in the α subunit of ENaC or a deletion or frameshift mutations in β and γ subunits of ENaC, rendering it unresponsive to aldosterone (33). Symptoms include weakness, fatigue, metabolic acidosis, vomiting and an inability to gain weight or grow at expected rates as well as extreme dehydration during infancy. Infants with systemic PHA-1 show more symptoms due to effects on multiple organs including cardiac arrhythmia, recurrent pulmonary infections and lesions under the skin (34).

Crohn's Disease is an inflammatory bowel disease (IBD) effecting the gastrointestinal tract. This occurs in any age range, although onset between 15 and 30 years of age is common. Symptoms include abdominal discomfort, diarrhea, intestinal stenosis, and extra intestinal complications. This has been associated with a deficiency of the γ subunit of ENaC leading to a lower reabsorption of sodium ions into the blood. If left untreated leads to a high risk of cancer at inflamed regions (35).

Cystic fibrosis (CF) is an autosomal recessive disease causing thick mucus to accumulate in the pulmonary system and gastrointestinal tract. Additionally, CF is associated with defects in the pancreas, liver, and kidneys (36). This is due to mutations in the cystic fibrosis transmembrane conductance regulator (CFTR) protein. CFTR is responsible for transporting chlorine across epithelial cells. A mutation in the α subunit of ENaC, W493R, and in the β subunit of ENaC have both been associated with cystic fibrosis. This is due to an increase of chlorine ions traversing intracellular space between epithelial cells which increase cAMP concentrations further inhibiting ENaC (37). This disease effects approximately 1 out of 300 newborns and 1 out of 25 adults are carriers, with no cure yet discovered (38).

The current project seeks to elucidate a purification scheme for the α subunit of ENaC using different combinations of buffers and lysis methods. Once purification is established, purified product will be subjected to Surface Plasmon Resonance (SPR) studies where interaction studies will be performed by flowing portions of the α subunit, β subunit, and γ subunit of the extracellular loop of ENaC, independently. This study seeks to identify critical interactions for formation of a functional heterotrimeric

channel which can then be used to elucidate pharmaceutical agents to aid in hypo/hypertension.

II. MATERIALS AND METHODS

A. Purification of α His2- α ENaC from *S. cerevisiae*

Cloning α His2- α ENaC for Yeast Expression

Polymerase chain reaction (PCR) reagents, cloning buffers, enzymes and NEB 5- α competent *E. coli* cells were purchased from New England Biolabs (Ipswich, MA). Plasmid DNA, pm α His2- α ENaC, was received from Dr. Jim Stockand (UTHSCSA, San Antonio, TX) which contained the gene for α ENaC with a 6X histidine tag (α His2) located in the extracellular loop region of α ENaC. Primers for PCR were previously designed against α ENaC and synthesized by Integrated DNA Technologies (Coralville, IA) (Table 1). EcoRI and NotI restriction sites were engineered on the ends of the primers in order for the gene to be subcloned into a yeast expression vector, pYES2/NTA, purchased from Life Technologies (Carlsbad, CA). PCR conditions were performed using 150 ng pm α His2- α ENaC template DNA, 1 μ M forward and reverse primer (Table 1), 400 μ M dNTPs, 1X Q5 Reaction Buffer, and 0.1 units of NEB Vent polymerase in a final reaction volume of 50 μ L. PCR instrument parameters started at 94 °C for 2 min followed by 25 cycles run at 94 °C for 30 s, 45 °C for 30 s, and 72 °C for 2 min with a final extension after the last cycle at 72 °C for 10 min. The PCR product was subjected to agarose gel electrophoresis and visualized with ethidium bromide to validate amplification of gene.

Table 1: PCR primers used.

Primer Name	Primer Sequence
α ENaC Forward (EcoRI)	5'-GCAAGAATTCTTATGCTGGACCACACCAC-3'
α ENaC Reverse (NotI)	5'-GCAAGCGGCCCGCCTCAGAGTGCCATGGC-3'

The PCR product (α His2- α ENaC) was cleaned and concentrated using the recommended protocol from DNA Clean & Concentrator™-5 kit from Zymo Research (Irvine, CA). The PCR product and the yeast expression vector, pYES2/NTA, were then subjected to restriction digest to create compatible sticky ends for ligation. Each digestion reaction, pYES2/NTA and PCR product, contained 1 X NEBuffer EcoRI, DNA (cleaned and concentrated α His2- α ENaC PCR product or 1.66 μ g pYES2/NTA plasmid DNA), 20 units of EcoRI and 20 units of NotI in a final reaction volume of 50 μ L. Digestion reactions were incubated for 1 hour at 37 °C before quenching the reaction with 1 X Endostop, a DNA loading buffer. Digestion products were run on a 0.7 % TAE agarose (w/v) gel and electrophoresis was run for 1.5 hours at 85 volts to resolve the DNA fragments.

The digestion products were gel extracted using QIAEX II Gel Extraction Kit and provided protocol from Qiagen (Venlo, Netherlands). Digestion products were quantitated to confirm purity and yields using the NanoDrop 2000 UV/Vis Spectrophotometer from Thermo Fisher Scientific (Waltham, MA). The insert and vector were ligated together in a 4:1 molar ratio (129.6 ng insert: 68.4 ng vector) with 1X T4 DNA Ligase Buffer and 400 units of T4 DNA Ligase in a 20 μ L reaction volume, in addition

to a vector-only negative control. For each ligation reaction 5 μ L were transformed into Top 10™ *E. coli* cells following a modified protocol from Chung and Miller (39). Top 10™ *E. coli* cells were thawed on ice for 10 minutes followed by an addition of cold KCM buffer (100 mM KCl, 30 mM CaCl₂, and 50 mM MgCl₂) at a 1:1 ratio along with ligation reaction. The transformation reaction was incubated on ice for 20 minutes followed by incubation in a room temperature water bath for 10 minutes. LB media was added to the transformation reaction and incubated at 37 °C with shaking at 225 rpm for 1 hour. The resulting solution was spread on LB plates containing ampicillin (100 μ g/mL) and incubated overnight at 37 °C. Two clones were picked from transformation plates and grown overnight shaking at 225 rpm at 37 °C in LB media containing ampicillin (100 μ g/mL). The cloned plasmid DNA was isolated using the QIAprep Spin Miniprep Kit from Qiagen with provided protocol with the exception of eluting with water as opposed to elution buffer. Cloned DNA was sequenced by Quintara Biosciences (Albany, CA) to verify ligation of insert into the vector. Verification was conducted by aligning the sequencing data with α ENaC using CLC Sequence Viewer from Qiagen.

Restriction digests were also conducted to confirm proper ligation using pYES2/NTA (negative control), pYES2/NTA/ α ENaC (positive control), and pYES2/NTA/ α His2- α ENaC. Each double digestion reaction contained 1 μ g of plasmid DNA, 1X Cutsmart™ buffer from New England Biolabs with 20 units of EcoRI and 20 units of NotI in a final reaction volume of 50 μ L. The reaction was incubated for 1 hour at 37 °C before quenching the reaction with 1 X Endostop. Digestion products were then subjected to agarose gel electrophoresis to analyze DNA fragments from the digestion.

Survival Dilution Growth “Pronging” Assay

S1 and BY4742 cells were transformed with pYES2/NTA (negative control), pYES2/NTA/LacZ, pYES2/NTA/ α ENaC, and pYES2/NTA/ α His2- α ENaC, separately, following the high efficiency lithium acetate transformation protocol. S1 and BY4742 yeast cells were grown overnight shaking at 225 rpm at 30 °C in YPDA media (1% w/v yeast extract, 2% w/v peptone, 2% w/v glucose, and 0.002% w/v adenine) and diluted the subsequent day to an OD₆₀₀ of 0.2. Yeast cultures were grown until an OD₆₀₀ of 0.4-0.6 was achieved. One milliliter of cells was pelleted by centrifugation at max speed for 1 min, discarding the supernatant. The following reagents were added to the remaining pellet in order; 240 μ L PEG 3350 (Mallinckrodt, St. Louis, MO), 36 μ L 1 M lithium acetate (Sigma-Aldrich, St. Louis, MO), 10 mg/mL sonicated salmon sperm DNA, heat activated at 96 °C for 10 min (Agilent Technologies, Santa Clara, CA), 0.45% β -mercaptoethanol (G Biosciences, St. Louis, MO), 1.5 μ g plasmid DNA and ddH₂O to a total volume of 360 μ L of transformation cocktail above the pellet. Transformation cocktail was vortexed for one minute followed by an incubation period of 20 min at 42 °C. Transformation cocktail was then centrifuged for 2 min at 2000 x *g*, supernatant discarded, and cell were resuspended in 200 μ L of ddH₂O. The transformed cells were then spread on synthetic media agar plates without uracil containing 2% w/v glucose and incubated at 30 °C for 2 days. Each cell strain was then placed in water at a 1/40 dilution. Each strain was sonicated for 8 sec at 3 amps and then counted using a hemacytometer and microscope. The cell concentration, 2×10^7 , was added to the first well of a 96-well plate and diluted in a 5-fold series across 6 wells. Dilutions were pronged onto synthetic selective media

plates without uracil containing ampicillin (100 µg/mL) with either 2% glucose or 2% galactose with and without additional 0.5 M NaCl and incubated at 30 °C for 3 days to show differences in growth and functionality of αHis2-αENaC versus the controls.

Yeast Expression

The sub-cloned product, pYES2/NTA/ αHis2-αENaC, pYES2/NTA/αENaC, and pYES2/NTA were transformed into S1 and BY4742 yeast strains separately following the high efficiency lithium acetate transformation protocol, described previously. Single colonies of each transformant, along with pYES2/NTA, were picked and grown in 50 mL synthetic media without uracil contain 2% glucose overnight shaking at 225 rpm at 30 °C. The OD₆₀₀ was measured the subsequent day and diluted to obtain an OD₆₀₀ = 0.2 in 250 mL of induction media (synthetic media without uracil containing 2% galactose). The cells were centrifuged (Beckman-Coulter Allegra™ 25R Centrifuge) for 5 min at 8000 *xg*, the supernatant was discarded, and cells resuspended in 250 mL of induction media. Cells were grown for 12 hours shaking at 225 rpm at 30 °C while taking 20 mL aliquots every two hours. Each two hour aliquot was centrifuged (Beckman-Coulter Allegra™ 25R Centrifuge) for 5 min at 8000 *xg* at 4 °C, discarding the supernatant. Pellets were resuspended in a volume of RIPA lysis buffer (150 mM NaCl, 1% Triton X-100, 1% sodium deoxycholate, 0.1% SDS, 2 mM PMSF, and 1X protease cocktail) that was 1% of the cell media spun down. An equal volume of 425-600 µm acid washed glass beads (Sigma-Aldrich, St. Louis, MO) to RIPA lysis buffer were added and vortexed for 8 minutes total

with 30 s intervals of vortexing and ice incubation to prevent overheating. Cell lysates were spun at 17,950 xg for 10 min and the supernatant was then collected and subjected to Pierce™ BCA Protein Assay Kit from Thermo Fisher Scientific (Waltham, MA) following supplied protocol. Cell lysate protein concentrations were determined from the assay and 50 μg of each 2 hour time aliquot containing 1X NuPAGE LDS sample buffer from Thermo Fisher Scientific (Waltham, MA) was heated at 90 °C for 10 min. Cell lysates were subjected to SDS-PAGE using a 4% stacking and a 7.5% resolving gel using PageRuler™ Prestained Protein Ladder from Thermo Fisher Scientific (Waltham, MA). The protein was transferred to a nitrocellulose membrane for western blot analysis using Trans-Blot® Turbo™ Transfer System from Bio-Rad (Hercules, CA) using parameters of 20 volts at constant 1.3 amps for 20 min. The membrane was then placed in blocking solution (1X TBS, 0.1% v/v Tween 20, and 5% w/v dry milk) for 30 minutes followed by a 5 min wash in 1X TBST. The membrane was then probed with mouse Anti-Xpress™ antibody (Life Technologies) using a dilution of 1:5000 in 1X TBST and incubated at 4 °C overnight while shaking. The subsequent day, the primary antibody was decanted and the membrane was washed three times in 1X TBST for 5 min each. The membrane was then probed with a secondary conjugated HRP goat anti-mouse antibody (Jackson ImmunoResearch, West Grove, PA) using a dilution of 1:1000 in 1X TBST shaking for one hour at room temperature. The secondary antibody was discarded and the membrane was washed three times in 1X TBST and a final wash in TBS, all for 5 min each. Western Lightning Plus ECL (Perkin Elmer, Waltham, MA) chemiluminescence substrate was used to detect α His2- α ENaC protein and imaged using ChemiDoc™ XRS+ System from Bio-

Rad Laboratories with a total exposure time of 5 min collecting images every 60 s. The membrane was stripped of antibodies using a stripping buffer (0.7% v/v BME, 2% v/v SDS, and 63 mM Tris, pH 8.0) and incubated at 55 °C followed by 5 washes with 10 mL of TBS. Once stripped, the membrane was probed again with Anti- α ENaC antibody from StressMarq Biosciences (Victoria, BC) at a 1:5000 dilution in blocking solution to confirm presence of α ENaC. The membrane was stripped again of antibodies, by the previously described method, and probed an additional time with an Anti- β -actin antibody from Santa Cruz Biotechnology (Dallas, TX) at a 1:1000 dilution in blocking solution.

Purification

Purification was performed using immobilized metal affinity chromatography (IMAC), with HisPur™ Ni-NTA Resin and 5 mL polypropylene columns from Pierce™ Thermo Fisher Scientific. S1 and BY4742 cell lysates containing α ENaC and α His2- α ENaC were independently immobilized on nickel resin after column was equilibrated with three column volumes equilibration buffer (0.3 M NaCl in 50 mM monobasic sodium phosphate, pH 8.0). Cell lysate flowthrough was collected and the column was washed with six column volumes of wash buffer (10 mM Imidazole with 0.3 M NaCl in 50 mM monobasic sodium phosphate, pH 8.0). Proteins were eluted with elution buffer (250 mM imidazole with 0.3 M NaCl in 50 mM monobasic sodium phosphate, pH 8.0) and 0.5 mL fractions were collected.

Purified protein fractions were quantitated by Pierce™ BCA Protein Assay Kit from Thermo Fisher Scientific (Waltham, MA) following supplied protocol. Protein concentrations were determined and 10 µg of protein sample were prepared and fractions were subjected to SDS-PAGE as previously described.

Purified protein fractions were then subjected to dialysis with Spectrapor® Membrane Tubing 3500 MW cut-off tubing. The proteins were placed in dialysis buffer (0.3 M NaCl in 50 mM monobasic sodium phosphate, pH 8.0) and stirred at 4 °C overnight, replacing the buffer one additional time the subsequent day.

B. Purification of ENaC peptides from *E. coli* for SPR

ENaC subunit peptides

Portions of each subunit of ENaC were previously sub-cloned into the bacterial expression vector pGEX-4T-2 (GE Healthcare, Pittsburgh, PA) by Grant Peltier (Table 2). The DNA of each subunit was cloned downstream of a glutathione S-transferase (GST) gene and a thrombin cleavage site to provide a method of purification and immobilizing peptides through anti-GST antibodies.

Table 2. Peptide sequences.

Peptide Name	Target Location	Peptide Sequence	# of Amino Acids	Predicate d Weight (Da)
N285	α -palm	EDTLGNFIFACRF <u>N</u> QVSCNQANYSHFH	27	3163.4
E438	β -thumb	NRDFPDWAHCYSDLQMSVAQR <u>E</u> TCIGMCKES	31	3622
E254	β -palm	SYPGEQMILACLFGA <u>E</u> PNCYRNFTSIFY	28	3235.6
Q444	γ -thumb	YQQHPNWMYCYQLHRA <u>F</u> VQEEELGCQSVCKEA	32	3953.4

Horizontal Gel Electrophoresis of ENaC oligonucleotides

BL21 *E. coli* cells with pGEX-4T-2 plasmid containing separately cloned ENaC portions E438, N285, E254, and Q444 were thawed and grown in 5 mL of LB media containing ampicillin shaking at 225 rpm overnight at 37 °C. The subsequent day plasmid DNA was isolated from clones using the QIAprep Spin Miniprep Kit from Qiagen and supplied protocol with the exception of eluting DNA from the spin column with water instead of elution buffer. Clones were then quantitated using the NanoDrop 2000 UV/Vis Spectrophotometer (Thermo Fisher Scientific). Clonal DNA, 441.3 ng, was loaded into a 0.7% TAE agarose (w/v) gel with a concentration of 1X loading dye and electrophoresis was run for 1 hour at 120 volts to ensure migration pattern of cloned insert into pGEX-4T-2.

Expression of GST- ENaC subunit peptides

Cloned plasmid DNA, 1 µg, was transformed into *E. coli* BL21 cells using the previously describe method. A full scale expression was conducted by placing the transformants in LB media containing ampicillin (100 µg/mL) overnight at 37 °C. Overnight cultures were added to 2X-YTG media containing ampicillin (100 µg/mL) and incubated at 37 °C for 3 hours shaking at 225 rpm. GST-peptides were induced by adding IPTG (Promega) at a final concentration of 0.1 mM and incubating at 37 °C for an additional 3 hours while shaking at 225 rpm. The resulting culture was centrifuged (Beckman-Coulter Allegra™ 25R Centrifuge) at 4600 xg for 5 minutes, discarding the supernatant.

The pellet was thawed in 1X PBS –Mg²⁺Ca²⁺ at a ratio of 0.05 to 1 mL of culture and was resuspended. The cells were lysed by conducting four freeze/thaw (-80 °C/ 22 °C) cycles. The cell lysate was treated with DNase 1 (Sigma Aldrich) and incubated at 37 °C for 30 minutes. The resulting cell lysate was centrifuged (Beckman-Coulter Allegra™ 25R Centrifuge) at 10500 xg for 20 minutes, retaining the supernatant.

The cell lysate was subjected to Pierce™ BCA Protein Assay Kit from Thermo Fisher Scientific (Waltham, MA) following supplied protocol. Cell lysate concentrations were calculated and 10 µg of each GST-peptide containing 1X NuPAGE LDS sample buffer from Thermo Fisher Scientific (Waltham, MA) were heated at 90 °C for 10 min. Cell lysates were subjected to SDS-PAGE using a 4% stacking and a 7.5% resolving gel

using PageRuler™ Prestained Protein Ladder from Thermo Fisher Scientific (Waltham, MA).

Purification

GST-peptides were purified by affinity chromatography using glutathione agarose resin from Pierce™ Thermo Fisher Scientific. Cell lysates were batch purified by adding 2 mL of glutathione agarose resin to each respected lysate and incubated on a rocker for 1 hour at 4 °C. The lysate was then added to a 5 mL polypropylene column from Pierce™ Thermo Fisher Scientific, allowing the resin to settle while collecting flow through fraction. The column was washed with 6 column volumes of 1X PBS-Mg-Ca followed by elution of GST-peptides using 3 mL of 10 mM reduced glutathione in 50 mM Tris-HCl pH 8, collecting three 1 mL fractions. The eluate was subjected back into the column, resuspending the glutathione agarose resin, and incubated for 10 minutes before collecting the final three 1 mL fractions, to increase amount of the GST-peptide bound to glutathione resin.

GST-peptides were dialyzed with Spectrapor® Membrane Tubing 3500 MW cut-off tubing. The GST-peptides were placed in dialysis buffer (20 mM Tris-HCl, pH 8.0) and stirred at 4 °C overnight, replacing the buffer one additional time the subsequent day. A 1 mL aliquot was saved after dialysis from each GST-peptide to use later for immobilization in SPR.

Thrombin Cleavage of GST-peptides

Glutathione agarose resin was regenerated for each respective peptide column by washing with 5 bed volumes of regeneration buffer 1 (0.5 M NaCl and 0.1% SDS in 0.1 M Tris-HCl, pH 8.5). The column was then washed with 5 bed volumes of ddH₂O followed by an additional wash with 5 bed volumes of regeneration buffer 2 (0.5 M NaCl and 0.1% SDS in 0.1 M sodium acetate, pH 4.5). A final wash with ddH₂O was conducted and stored with 1X PBS-Mg-Ca at 4 °C.

Dialyzed GST-peptides were subjected to regenerated glutathione columns shaking at room temperature for 1 hour. The column was washed with 3 column volumes of 1X PBS-Mg²⁺-Ca²⁺ and incubated overnight, at room temperature, while shaking in thrombin reaction mixture (1:20 ratio of 35 units of Thrombin to 1X PBS-Mg-Ca). The eluate was collected and thrombin was separated from cleaved peptides by subjecting eluate to 1 ml *p*-AminoBenzamidine agarose resin (Sigma Aldrich) in a 5 mL polypropylene column from Pierce™ Thermo Fisher Scientific. The resin was previously washed with 3 bed volumes of Tris Buffer (0.4 M NaCl in 50 mM Tris-HCl, pH 8.15) to equilibrate the resin. The cleaved peptides were subjected to the column and incubated overnight while shaking at 4 °C. The subsequent day the cleaved peptides were eluted with Tris buffer, collecting in 0.5 mL fractions.

Quantitation of Peptides

Cleaved peptides were quantitated from measuring the absorbance at 280 nm with BIO-RAD SmartSpec™ 3000 and solved using the tryptophan/tyrosine extinction coefficient concentration equation:

$$C = \frac{A_{280} \times DF \times MW}{(\#W \times 5560 \text{ L mol}^{-1}\text{cm}^{-1}) + (\#Y \times 1200 \text{ L mol}^{-1}\text{cm}^{-1})}$$

where A_{280} is the absorbance at 280 nm, DF is the dilution factor, MW is the molecular weight in mg/mmmole, #W is the number of tryptophan residues, 5560 is the extinction coefficient of tryptophan at 280 nm at a neutral pH in a 1 cm cell with units of AU/mmmole/mL, #Y is the number of tyrosine residues, 1200 is the extinction coefficient of tyrosine at 280 nm at a neutral pH in 1 cm cell with units of AU/mmmole/mL. An additional method for peptide quantitation employed Pierce™ Quantitative Colorimetric Peptide Assay from Thermo Fisher Scientific following supplied protocol.

C. SPR Analysis

Binding Assays

Binding assays were conducted by SPR on a Biacore® X (GE Healthcare). The binding assays were performed with 0.4 M NaCl in 50 mM Tris-HCl, pH 8.15 at 5 μ L/min. Peptide analytes were injected at increasing concentrations at 50 μ L sample size. Kinetic data calculations were performed using BIAevaluation software version 2.3.

CM5 Chip Setup

All reagents for activation of the CM5 chip were provided from GE Healthcare's Amine Coupling Kit and GST Capture Kit. The CM5 chip was activated on both flow cells with a 1:1 EDC/NHS solution injection of 35 μL injection at 5 $\mu\text{L}/\text{min}$ with a 7 minute contact time. Anti-GST was diluted to 15 $\mu\text{g}/\text{mL}$ with an injection of 25 μL for a 5 minute contact time. The remaining activated NHS-esters are deactivated/blocked with a 35 μL injection ethanolamine for a 7 minute contact time. High affinity sites on anti-GST were blocked by injecting 15 μL of a 5 $\mu\text{g}/\text{mL}$ recombinant GST for a 3 minute contact time. Only one flow cell was regenerated with a 10 μL injection for a 2 minute contact time, leaving the remaining flow cell as a reference.

All GST-peptides (Table 2) were immobilized onto the CM5 through GST-antibody interactions. GST-peptide binding assays were performed with their counterpart analyte with the exception that αENaC and $\alpha\text{His2-}\alpha\text{ENaC}$ analytes were assayed over all four GST-peptides (Table 3).

Table 3. Concentrations of peptide/protein injections and interactions with immobilized peptide.

GST-Peptide Analyte Interaction	Concentrations Injected
GST-E438---N285 & GST N285---E438	90 $\mu\text{g}/\text{mL}$, 150 $\mu\text{g}/\text{mL}$, 250 $\mu\text{g}/\text{mL}$, 359 $\mu\text{g}/\text{mL}$
GST-E254---Q444 & GST-Q444---E254	5.8 $\mu\text{g}/\text{mL}$, 11.5 $\mu\text{g}/\text{mL}$, 23.1 $\mu\text{g}/\text{mL}$, 46.2 $\mu\text{g}/\text{mL}$
[GST-E438, GST-N285, GST-E254, GST-E254]--- αENaC	1.25 $\mu\text{g}/\text{mL}$, 2.5 $\mu\text{g}/\text{mL}$, 5 $\mu\text{g}/\text{mL}$, 10 $\mu\text{g}/\text{mL}$
[GST-E438, GST-N285, GST-E254, GST-E254]--- αHis2	1.25 $\mu\text{g}/\text{mL}$, 2.5 $\mu\text{g}/\text{mL}$, 5 $\mu\text{g}/\text{mL}$, 10 $\mu\text{g}/\text{mL}$

III. RESULTS AND DISCUSSION

To study the location of interaction between the subunits of ENaC, purification and SPR studies were performed to determine K_A and K_D values of the full length alpha subunit of ENaC interacting with peptide portions of each subunit of ENaC. This information could be used to perform site specific mutagenesis studies to elucidate if a residue is critical for proper association and dissociation as well as to perform similar studies but with ENaC peptides upstream and downstream of the currently studied ENaC peptide. In these studies, gene encoding for the alpha subunit of ENaC containing a 6X histidine tag (α His2- α ENaC), located in the extracellular loop region, was subcloned into a yeast expression vector and expressed. This was followed by survival growth studies, purification of native α ENaC as well as α His2- α ENaC, and SPR studies to determine K_D and K_A values of ENaC peptides with the full subunit α ENaC.

A. Purification of α His2- α ENaC from *S. cerevisiae*

Cloning α His2- α ENaC for Yeast Expression

α His2- α ENaC gene was amplified by PCR from pm α His2- α ENaC, a mammalian expression vector (donated by the Stockand lab, UTHSCSA). The PCR products were approximately 2 kb in size and compared to a control reaction containing no template DNA (FIG 7). The α ENaC gene from *Mus musculus* is 2238 bp and with the addition of a 6x histidine tag located in the extracellular loop, α His2, provide the 2.3 kb fragment seen in gel electrophoresis (FIG 7).

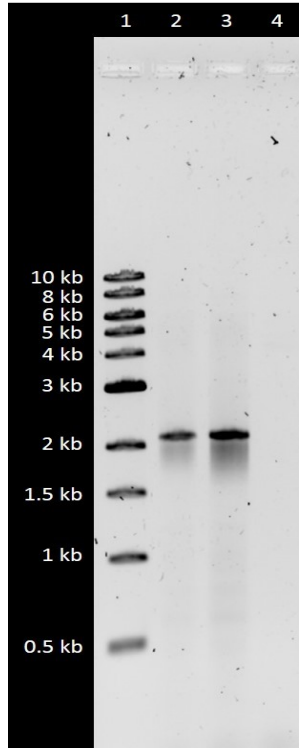


FIG 7. Polymerase Chain Reaction (PCR) of α His2- α ENaC gene from p α His2- α ENaC plasmid DNA. The gene was amplified and run on a 0.7% w/v TAE agarose gel to verify the reaction. *lane 1*, 1 kb DNA ladder. *lane 2-3*, α His2- α ENaC amplification. *lane 4*, negative control with no p α His2- α ENaC template DNA. The gel was stained with ethidium bromide and the image color was inverted.

The α His2- α ENaC PCR product along with pYES2/NTA, yeast expression vector, were digested with restriction enzymes EcoRI and NotI. The restriction digest produced compatible sticky ends on α His2- α ENaC PCR product and on pYES2/NTA multiple cloning site (MCS) for ligation of insert gene. The restriction digest products were run on a 0.7% w/v TAE agarose gel to define appropriate DNA fragments for excision from the gel (FIG 7). The α His2- α ENaC PCR product, 2.3 kb, and the pYES2/NTA yeast expression vector, 6 kb, were extracted from the gel (FIG 8).

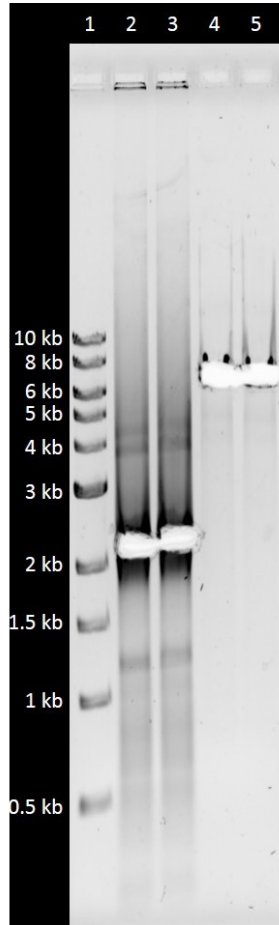


FIG 8. Gel extraction of digested α His2- α ENaC PCR product and digested pYES2/NTA plasmid DNA. Digested α His2- α ENaC PCR product and digested pYES2/NTA were separated on a 0.7% w/v TAE agarose gel and gel extracted. *lane 1*, 1 kb DNA ladder. *lane 2-3*, α His2- α ENaC PCR digestion product. *lane 4-5*, pYES2/NTA digestion product. The gel was stained with ethidium bromide and the image color was inverted.

The α His2- α ENaC gene migrated approximately 2.2 kb and the yeast expression vector, pYES2/NTA, migrated approximately 6.1 kb. The bands were gel extracted separately, cleaned, concentrated and quantitated using Qiagen QIAEX II Gel Extraction Kit (FIG 8), DNA Clean & Concentrator™-5 (Zymo Research), and the NanoDrop2000 UV/vis Spectrophotometer (ThermoFisher Scientific) respectively. DNA fragments were ligated using a 4:1 molar ratio of gene insert to yeast expression vector, keeping total DNA in ligation reaction at 200 ng, for 10 minutes at room temperature using T4 DNA

ligase (New England Biolabs) in 1X T4 DNA ligase buffer. After room temperature incubation, the ligation reaction was transformed into Top 10™ *E. coli* cells following a protocol from Chung and Miller (31), plated on LB containing ampicillin plates, selecting for transformants expressing an ampicillin resistant gene, and grown overnight at 37 °C.

Once the ligation reaction was transformed into Top 10™ *E. coli*, pYES2/NTA/αHis2-αENaC was isolated from a bacterial cell culture using QIAprep Spin Miniprep Kit (Qiagen). To confirm that the αHis2-αENaC gene was properly cloned, a pYES2/NTA/αHis2-αENaC (8.2 kb) restriction map was created and analyzed using NEBcutter® from New England Biolabs website. The restriction enzymes EcoRI and NotI were predicted to cut pYES2/NTA/αHis2-αENaC into two fragments of approximately 6 kb and 2.2 kb. pYES2/NTA/αHis2-αENaC, as well as restriction digestion product, were run on a 0.7% w/v TAE agarose gel (FIG 8). The uncut pYES2/NTA, yeast expression vector (6 kb), migrated approximately 4 kb and the restriction-digested pYES2/NTA reaction created a band that migrated approximately 6 kb (FIG 8, lanes 2 and 3). The uncut pYES2/NTA/αENaC (8 kb) migrated approximately 6 kb and the restriction digested pYES2/NTA/αENaC reaction created two fragments, one being the linear pYES2/NTA vector migrating approximately 6 kb and the second band being the αENaC gene migrating approximately 2 kb (FIG 9, lanes 4 and 5). The uncut pYES2/NTA/αHis2-αENaC plasmid (8 kb) migrated approximately 6 kb (FIG 9, lanes 6 and 8) and the restriction digested pYES2/NTA/αHis2-αENaC reaction created two bands, one being the pYES2/NTA vector migrating approximately 6 kb and the second band being the αHis2-αENaC gene migrating approximately 2 kb (FIG 9, lanes 7 and 9). Differences between

the controls, pYES2/NTA and pYES2/NTA/ α ENaC, compared to pYES2/NTA/ α His2- α ENaC are due to the plasmid DNAs conformations, seen in a supercoiled form as opposed to a linear form or nicked open circular form, which migrate at slower rates due to its topology and hydrodynamic radius. (32). The digestion products of pYES2/NTA/ α His2- α ENaC compared to pYES2/NTA/ α ENaC ran as expected with each of their bands at 6 kb and 2.2 kb, indicating that the α His2- α ENaC was cloned in (FIG 9, lane 5, lanes 7 and 9). An increase shift in the migration pattern between the 2 kb band of α His2- α ENaC when compared to α ENaC was not expected based on the 18 nt difference from the 6X histidine tag (FIG 9, Lane 5, lanes 7 and 9). The pYES2/NTA/ α His2- α ENaC plasmid was sequenced by Quintara Biosciences. A sequence alignment was created using CLC Sequence Viewer program, available from Qiagen Bioinformatics website, to identify inaccuracies and verify the 6X histidine tag was present between the α ENaC and α His2- α ENaC genes.

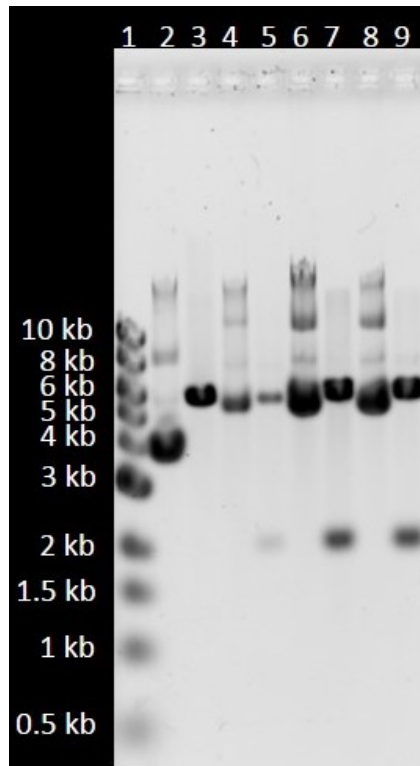


FIG 9. pYES2/NTA/ α ENaC plasmid isolation and digestion from Top 10™ *E. coli* cells to verify cloning. The ligation reaction as transformed into Top 10™ *E. coli* cells and plasmid DNA was isolated from 2 transformant colonies prior to sequencing. *lane 1*, 1 kb DNA ladder. *lane 2*, pYES2/NTA yeast expression vector. *lane 3*, pYES2/NTA yeast expression vector digested with EcoRI and NotI. *lane 4*, pYES2/NTA/ α ENaC. *lane 5*, pYES2/NTA/ α ENaC digested with EcoRI and NotI. *lane 6*, pYES2/NTA/ α His2- α ENaC plasmid DNA from clone 1. *lane 7*, pYES2/NTA/ α His2- α ENaC clone 1 digested with EcoRI and NotI. *lane 7*, pYES2/NTA/ α ENaC digested with EcoRI and NotI. *lane 8*, pYES2/NTA/ α His2- α ENaC plasmid DNA from clone 2. *lane 9*, pYES2/NTA/ α His2- α ENaC clone 2 digested with EcoRI and NotI. The gel was stained with ethidium bromide and the image color was inverted.

Survival Dilution Growth “Pronging” Assay

The plasmids pYES2/NTA, pYES2/NTA/LacZ, pYES2/NTA/ α ENaC, and pYES2/NTA/ α His2- α ENaC were transformed into yeast strains BY4742 and S1 using the high efficiency lithium acetate transformation protocol described previously. A survival dilution assay was conducted to verify the functionality of α ENaC to α His2 to ensure the 6X histidine tag was not altering functionality of this modified α ENaC. The cells were

plated on synthetic media without uracil containing ampicillin and either 2% glucose, *GAL1* promoter is suppressed, 2% galactose, *GAL1* promoter is unoccupied, and in the presence of excess salt, 0.5 M (FIG 10 and 11).

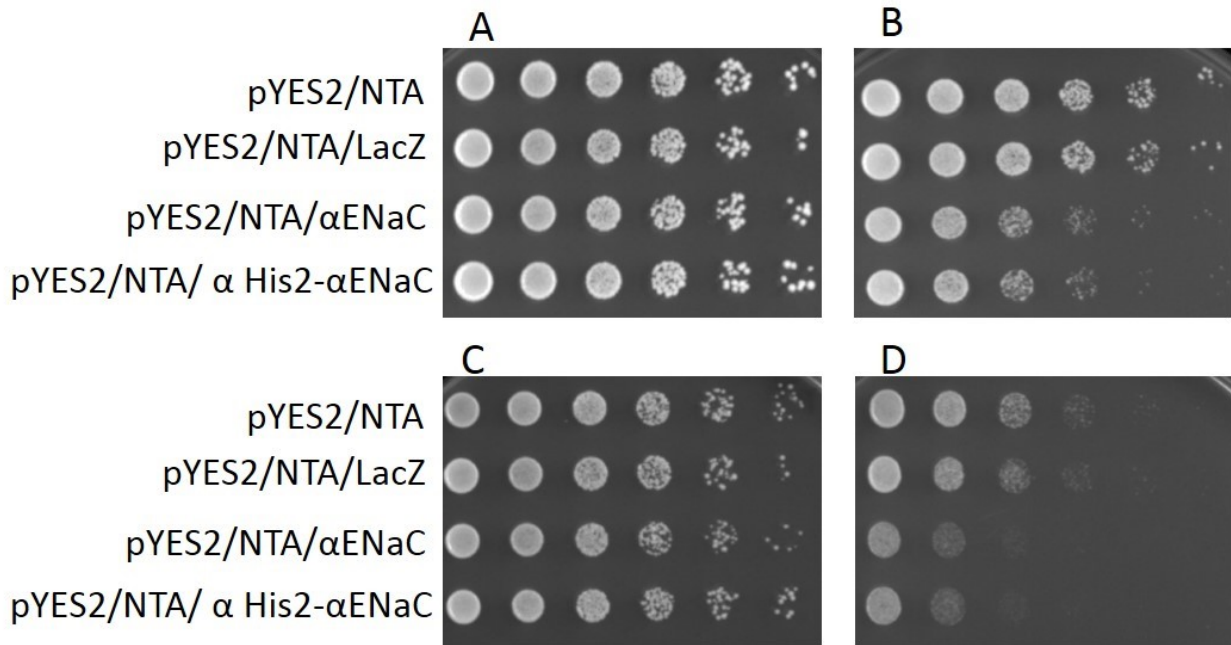


FIG 10. Survival dilution growth "pronging" assay in BY4742 yeast cells. pYES2/NTA, pYES2/NTA/LacZ, pYES2/NTA/αENaC, and pYES2/NTA/αHis2-αENaC were transformed into BY4742 yeast cells and plated to detect salt sensitivity compared to the controls. **A** – Cells grown on synthetic media without uracil containing 2% glucose. **B** – Cells grown on synthetic media without uracil containing 2% galactose. **C** – Cells grown on synthetic media without uracil containing 2% glucose and 0.5 M NaCl. **D** – Cells grown on synthetic media without uracil containing 2% galactose and 0.5 M NaCl.

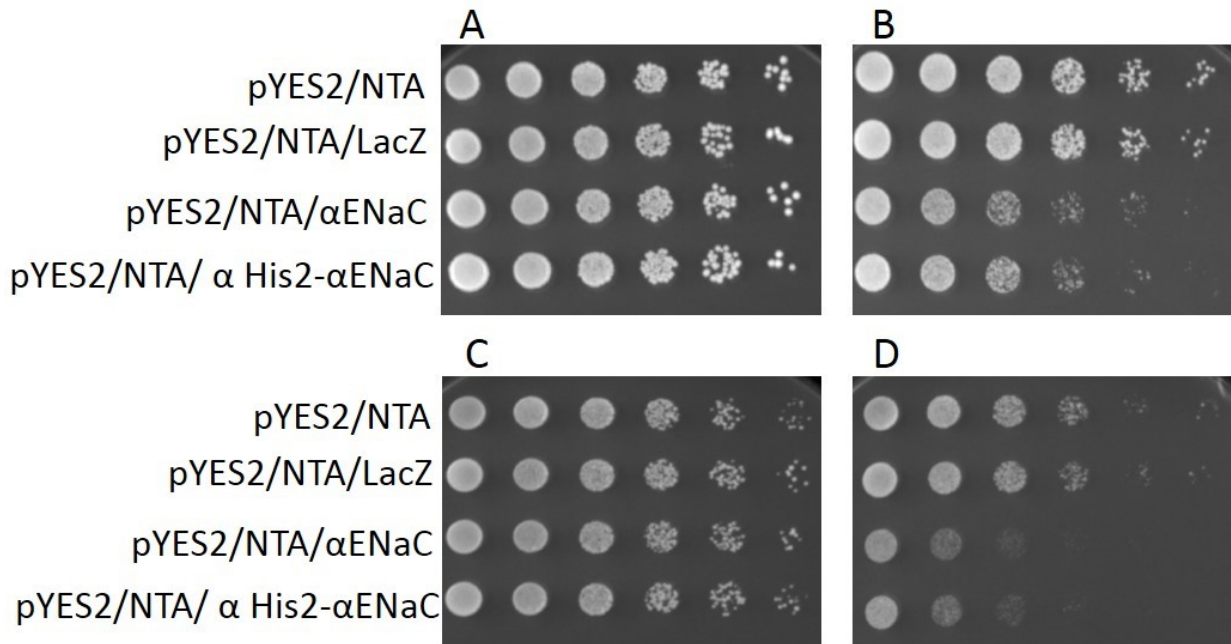


FIG 11. Survival dilution growth “pronging” assay in S1 yeast cells. pYES2/NTA, pYES2/NTA/LacZ, pYES2/NTA/αENaC, and pYES2/NTA/αHis2-αENaC were transformed into S1 yeast cells and plated to detect salt sensitivity compared to the controls. **A** – Cells grown on synthetic media without uracil containing 2% glucose. **B** – Cells grown on synthetic media without uracil containing 2% galactose. **C** – Cells grown on synthetic media without uracil containing 2% glucose and 0.5 M NaCl. **D** – Cells grown on synthetic media without uracil containing 2% galactose and 0.5 M NaCl.

In comparing the functionality of αENaC to αHis2-αENaC between yeast strains, BY4742 and S1, they experienced similar growth inhibition without and in the presence of excess salt (0.5 M) between non-expressive media, 2% glucose, and expressive media, 2% galactose (FIG 10-11). When compared to the controls αENaC and αHis2-αENaC experienced greater growth inhibition which was expected due to the lack of the yeast cells able to transport sodium into the cytoplasm without αENaC (FIG 10-11).

Yeast Cell Lysis Screen

In order to purify α His2- α ENaC a yeast cell lysis screen was conducted, along with a α ENaC control, to elucidate which lysis method and buffer conditions would be ideal for purification. Eight, 20 milliliter samples of α His2- α ENaC were induced for 8 hours, as previously described. Alkaline lysis is a harsh chemical treatment to lyse yeast cells. It is similar to SDS sample buffer however it contains a final concentration of 100 mM NaOH, to help break open the cell wall. Proteins that undergo this process are not able to be further purified due to treatment of the whole cell lysate, it was conducted here as a positive control. α ENaC ran approximately 100 kDa similar to that of α His2- α ENaC and also contain another band at approximately 35 kDa which most likely is degradation of the protein (FIG 12, lanes 2-3). An additional band could be seen at approximately 99 kDa which is due to glycosylation of α ENaC (FIG 12, lanes 2-9). Also, the signal for α ENaC was more intense than that of α His2- α ENaC which could be attributed to the lysis method itself (FIG 12, lanes 2-3). Acid washed glass beads, 425-600 μ m in size, were used along with a monobasic sodium phosphate buffer pH 7.4. However, the intensity of α ENaC and α His2- α ENaC bands are very faint, migrating approximately 100 kDa with the absence of second glycosylation product band (FIG 12, lanes 4-5). The alternative lysis buffer used with the acid washed glass beads was a RIPA buffer. This buffer contains sodium deoxycholate, an ionic detergent, and Triton X-100, a non-ionic detergent. These two chemicals help solubilize the membrane and due to their nature, help stabilize the hydrophilic and hydrophobic portions of α ENaC. α ENaC and α His2- α ENaC ran approximately 100 kDa with the presence of a second glycosylated

product band at approximately 99 kDa (FIG 12, lanes 6-7). Lysis by sonication was conducted in the presence of a NaH_2PO_4 buffer which applies ultrasonic frequencies to the sample causing the formation and collapse of microspheres which creates shear force to break cell walls. αENaC and $\alpha\text{His2-}\alpha\text{ENaC}$ ran at approximately 100 kDa with the presence of a second glycosylation product band at approximately 99 kDa. However the signal intensity of the former was higher than latter (FIG 12, lanes 8-9). When comparing the different lysis methods and buffer conditions tested, the acid washed glass beads with RIPA buffer was chosen for further purification studies (FIG 12).

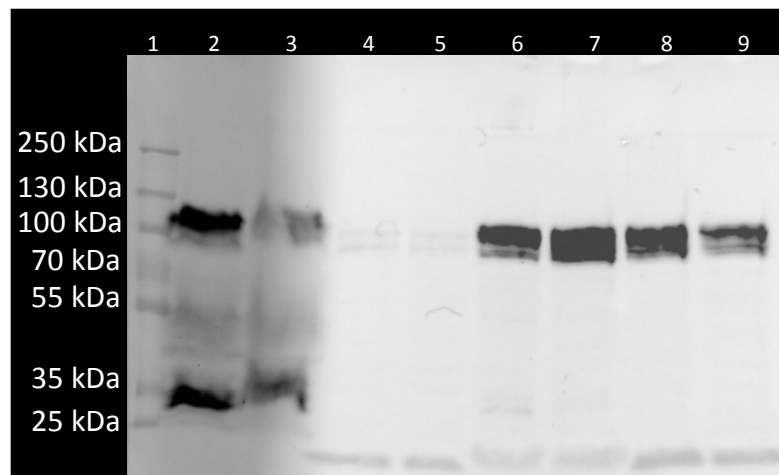


FIG 12. Western blot analysis of $\alpha\text{His2-}\alpha\text{ENaC}$ using different lysis conditions. pYES2/NTA/ αENaC and pYES2/NTA/ $\alpha\text{His2-}\alpha\text{ENaC}$ plasmids were transformed into S1 yeast cells and different lysis conditions were performed to identify an optimal method for protein extraction. Total protein of each sample was 50 μg . Membrane was probed with primary anti-Xpress™ antibody followed by probing with a secondary goat anti-mouse antibody conjugated with HRP. *lane 1*, PageRuler™ Plus Prestained protein ladder. *lane 2*, alkaline lysis of αENaC . *lane 3*, alkaline lysis of $\alpha\text{His2-}\alpha\text{ENaC}$. *lane 4*, Glass bead lysis of αENaC in NaH_2PO_4 . *lane 5*, Glass bead lysis of $\alpha\text{His2-}\alpha\text{ENaC}$ in NaH_2PO_4 . *lane 6*, Glass bead lysis of αENaC in RIPA. *lane 7*, Glass bead lysis of $\alpha\text{His2-}\alpha\text{ENaC}$ in RIPA. *lane 8*, Sonication αENaC in NaH_2PO_4 . *lane 9*, Sonication of $\alpha\text{His2-}\alpha\text{ENaC}$ in NaH_2PO_4 .

Yeast Expression

BY4742 and S1 yeast cells containing pYES2/NTA, empty vector (EV) control, and pYES2/NTA/ α His2- α ENaC were expressed in yeast independently to confirm protein production in each strain. Each sample was grown for 16 hours in synthetic media without uracil containing 2% glucose and an OD₆₀₀ was measured to determine cell density. The samples were then back diluted down to an OD₆₀₀ of 0.2 in expression synthetic media without uracil contain 2% galactose. Twenty milliliter aliquots were collected every two hours for a total time of 12 hours. The aliquots were centrifuged, the supernatant was discarded and the samples were resuspended in RIPA buffer containing PMSF and EDTA-free protease cocktail. Acid washed glass beads were added to the cell suspension and vortexed to lyse the cells. Cellular debris was removed through centrifugation and total protein of cell lysates was quantitated through a BCA assay. Equal protein amounts, 50 μ g, of each sample, along with its control, were run on a 7.5% SDS-PAGE and transferred to a nitrocellulose membrane.

Western blot analysis was conducted to verify the expression of α His2- α ENaC protein as well as the optimal time to harvest the protein for purification. The empty vector was used as a negative control to demonstrate α His2- α ENaC protein expression was absent. α ENaC has an approximate molecular weight of 78 kDa however it has been seen that glycosylation can increase this anywhere from 15 – 20 kDa as well as the 6X histidine tag on α His2- α ENaC giving it an approximate molecular weight of 100 kDa (FIG 13 A, B & FIG 14 A, B). β -actin is a 42 kDa protein responsible for cell motility, structure, and integrity and was used here as a positive control for cell lysis (FIG 13 C - FIG 14 C).

α His2- α ENaC was expression was detected by Anti-Xpress™ antibody after 1 minute of exposure (FIG 13 A - FIG 14 A). Multiple bands can be seen in 4 of the 7 lanes in Figure 13A (lanes 12-15) and in Figure 14A (lanes 11-15). This is attributed to variations of glycosylation as well as degradation of α His2- α ENaC. The nitrocellulose membrane was stripped of antibodies and probed with anti- α ENaC antibody and imaged as previously (FIG 13B - FIG 14B). The anti- α ENaC antibody sensitivity decreased greatly in Figure 13 B (lanes 12-15) and slightly in Figure 14 B (lanes 11-15) while detecting a very high background signal in all lanes of Figures 13 B and 14 B. This is likely due to specificity of the anti- α ENaC antibody when compared to the Anti-Xpress™ antibody since the latter antibody is specific to an epitope engineered into the expression vector. Also, the stripping method is harsh and can cause degradation of proteins on the nitrocellulose membrane. The specificity of each antibody can also be seen when comparing α His2- α ENaC in Figure 13 (lanes 9-15) and in Figure 14 (lanes 9-15) to the empty vector control in Figure 13 (lanes 2-8) and in Figure 14 (lanes 2-8) with a much higher non-specific background reading in the latter figure. To confirm the lysis method worked accurately the nitrocellulose membrane was stripped again and probed with anti- β -actin antibody and imaged as previously (FIG 13 C – FIG 14 C). Due to the S1 yeast strains total protein concentration of cell lysate and higher signal readings from western blot analysis, purification of the α His2- α ENaC will be conducted from only this yeast strain.

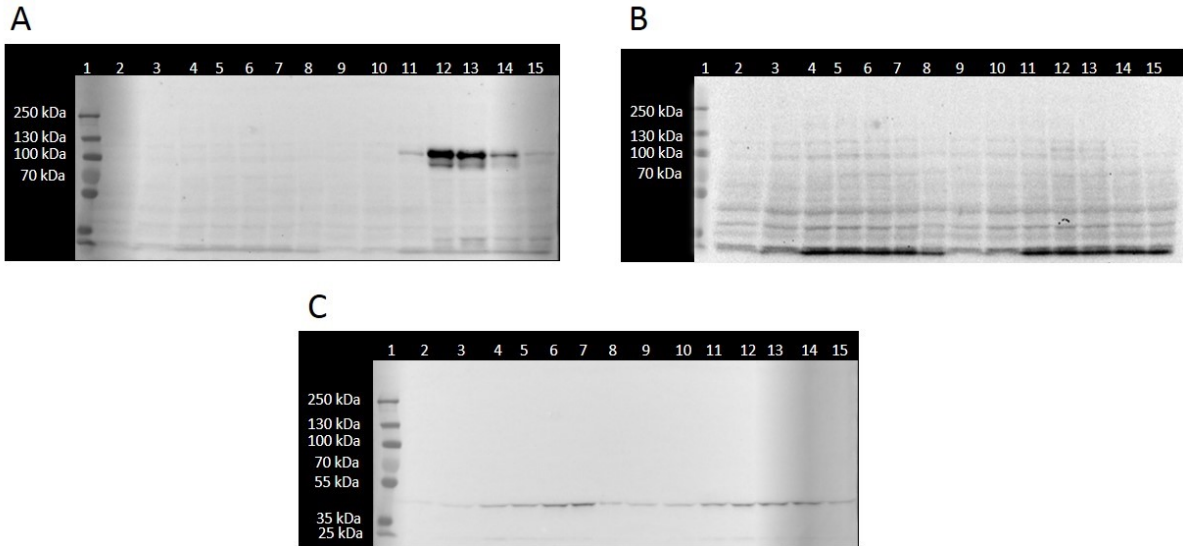


FIG 13. Western blot analysis of α His2- α ENaC time course in BY4742 yeast strain. pYES2/NTA and pYES2/NTA/ α His2- α ENaC plasmids were transformed into BY4742 yeast cells for a time course expression of α His2- α ENaC protein to identify optimal time for protein harvest. Total protein of each sample was 50 μ g. **A** – Blot probed with Anti-Xpress™ antibody (1:5000 dilution). **B** – Blot probed with anti- α ENaC antibody (1:1000 dilution). **C** – Blot probed with anti- β -actin antibody (1:1000 dilution) as a control. *lane 1*, PageRuler™ Plus Prestained protein ladder. *lane 2*, EV T= 0. *lane 3*, EV T= 2. *lane 4*, EV T= 4. *lane 5*, EV T=6. *lane 6*, EV T= 8. *lane 7*, EV T= 10. *lane 8*, EV T= 12. *lane 9*, α His2- α ENaC T= 0. *lane 10*, α His2- α ENaC T= 2. *lane 11*, α His2- α ENaC T= 4. *lane 12*, α His2- α ENaC T= 6. *lane 13*, α His2- α ENaC T= 8. *lane 14*, α His2- α ENaC T= 10. *lane 15*, α His2- α ENaC T= 12.

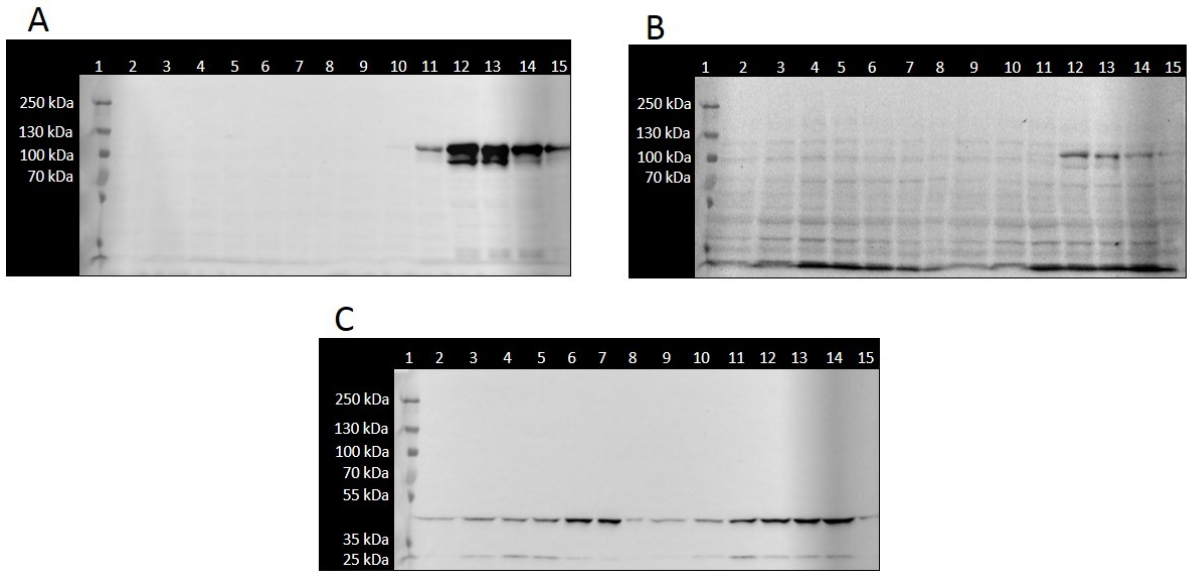


FIG 14. Western blot analysis of α His2- α ENaC time course in S1 yeast strain. pYES2/NTA (EV) and pYES2/NTA/ α His2- α ENaC plasmids were transformed into S1 yeast cells for a time course expression of α His2- α ENaC protein to identify optimal time for protein harvest. Total protein of each sample was 50 μ g. **A** – Blot probed with Anti-Xpress™ antibody (1:5000 dilution). **B** – Blot probed with anti- α ENaC antibody (1:1000 dilution). **C** – Blot probed with anti- β -actin antibody (1:1000 dilution) as a control. *lane 1*, PageRuler™ Plus Prestained protein ladder. *lane 2*, EV T= 0. *lane 3*, EV T= 2. *lane 4*, EV T= 4. *lane 5*, EV T=6. *lane 6*, EV T= 8. *lane 7*, EV T= 10. *lane 8*, EV T= 12. *lane 9*, α His2- α ENaC T= 0. *lane 10*, α His2- α ENaC T= 2. *lane 11*, α His2- α ENaC T= 4. *lane 12*, α His2- α ENaC T= 6. *lane 13*, α His2- α ENaC T= 8. *lane 14*, α His2- α ENaC T= 10. *lane 15*, α His2- α ENaC T= 12.

Purification

Purification was performed via immobilized metal affinity chromatography (IMAC) by passing through whole cell lysate, containing α His2- α ENaC, through a nickel affinity column to allow for the 6X histidine tag of α His2- α ENaC to interact with the nickel resin. α His2- α ENaC was noticed in the flow through, running approximately 100 kDa, indicating not all of it was captured by the nickel column (FIG 15 lane 2). The bound α His2- α ENaC was washed with 10 mM imidazole and 0.3 M NaCl in 50 mM NaH_2PO_4 , pH 8.0 which further removed any remaining proteins weakly interacting with the nickel

resin (FIG 15, lane 3). Bound α His2- α ENaC was eluted with 250 mM imidazole and 0.3 M NaCl in 50 mM NaH_2PO_4 , pH 8.0 (FIG 15, lanes 4-10). α His2- α ENaC ran approximately 100 kDa seen throughout Figure 15. However, the presence of higher bands produced a signal most likely due to aggregation of the protein into a larger complex as well as lower bands most likely caused by degradation of α His2- α ENaC protein (FIG 15). The flow through still contained α His2- α ENaC protein seen in Figure 15 (lane 2) and can be contributed to a high cell lysate concentration to nickel resin ratio where cellular proteins were also competing to interact with the nickel resin. α His2- α ENaC is also present in the wash (FIG 15, lane 3) however at much lower intensity which was expected since the wash buffer contained a low concentration of imidazole. However, with the slight overlap of collecting samples it most likely seems the flow through was present in the wash (FIG 15, lane 2) and consequently the wash comprised most of fraction 1 (FIG 15, lane 3). α His2- α ENaC was eluted in fraction 2 as well as fraction 4 (Fig 15, lane 5,7). These fractions were quantitated via a BCA assay prior to being used for SPR and resulted in fraction 2 (FIG 15, lane 2) with a total protein content of 682 μg and fraction 4 (FIG 15, lane 4) with a total protein content of 234 μg .

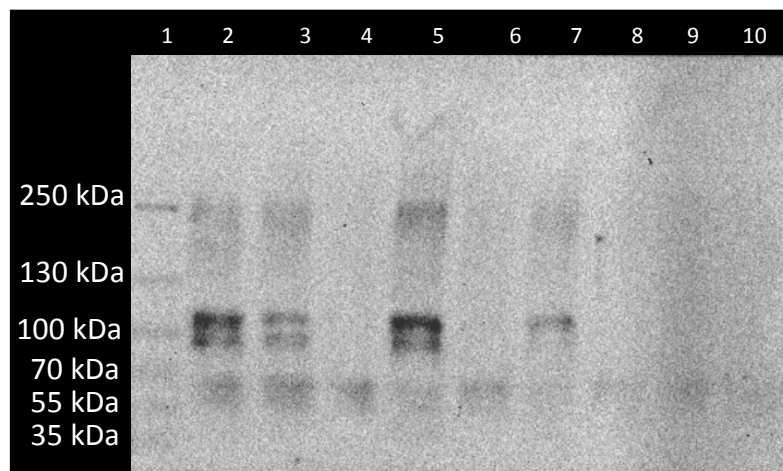


FIG 15. IMAC purification of α His2- α ENaC analyzed by western blotting. pYES2/NTA/ α His2- α ENaC plasmid were transformed into S1 yeast cells and purified via a nickel affinity column. Total protein of each sample was 10 μ g. Membrane was probed with primary anti-Xpress™ antibody followed by probing with a secondary goat anti-mouse antibody conjugated with HRP. *lane 1*, PageRuler™ Plus Prestained protein ladder. *lane 2*, Cell lysate flow through. *lane 3*, Nickel column wash. *lane 4*, fraction 1 of α His2- α ENaC. *lane 5*, fraction 2 of α His2- α ENaC. *lane 6*, fraction 3 of α His2- α ENaC. *lane 7*, fraction 4 of α His2- α ENaC. *lane 8*, fraction 5 of α His2- α ENaC. *lane 9*, fraction 6 of α His2- α ENaC. *lane 10*, fraction 7 of α His2- α ENaC.

B. Purification of ENaC peptides from *E. coli* for SPR

Horizontal Gel Electrophoresis of ENaC peptides

ENaC peptide ligands were previously cloned into the pGEX-4T-2 bacterial expression vector and transformed into BL21 (DE3) pLysS cells seen in Table 4 (40). The bacterial cells containing the ENaC ligand plasmids were grown in TB overnight at 37 °C and the plasmids were isolated separately as previously described. The isolated plasmids were quantitated and 0.7% w/v TAE agarose gel electrophoresis was conducted to ensure correct migration pattern from previous results (40).

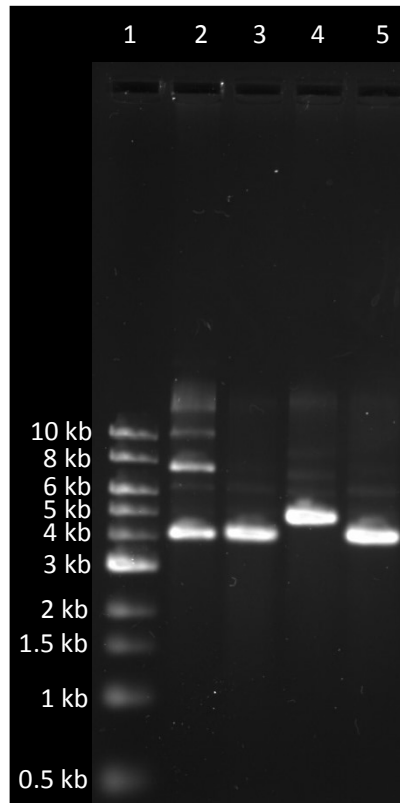


FIG 16. Plasmid isolation of ENaC ligand genes. pGEX-4T-2/E254, pGEX-4T-2/N285, pGEX-4T-2/E438, and pGEX-4T-2/Q444 were isolated separately from BL21 *E. coli* cells and run on a 0.7% w/v TAE agarose gel to verify each ENaC ligand. *lane 1*, 1 kb DNA ladder. *lane 2*, pGEX-4T-2/E254. *lane 3*, pGEX-4T-2/N285. *lane 3*, pGEX-4T-2/E438. *lane 4*, pGEX-4T-2/Q444. The gel was stained with ethidium bromide.

Table 4. ENaC peptides and their location.

<u>Ligand</u>	<u>Sequence</u>	<u># of Amino Acids</u>	<u>Predicted Weight</u>	<u>Location</u>
E438	NRDFPDWAHCYSDLQMSVAQRETCIGMCKES	31	3622	β -thumb
N285	EDTLGNFIFACRFNQVSCNQANYSHFH	27	3163.4	α -palm
E254	SYPGEQMILACLFGAEPNRYNFTSIFY	28	3235.6	β -palm
Q444	YQQHPNWMYCYQLHRAFVQEELGCQSVCKEA	32	3953.4	γ -thumb

The empty bacterial expression vector, pGEX-4T-2, is 4,970 bp in size and due to the small size of the ENaC ligands, there will be a non-noticeable shift in migration. pGEX-4T-2/E254 migrated approximately 4.1 kb which was expected due to the size of the expression vector and E254, 24 nt (FIG 16, lane 2). pGEX-4T-2/N285 migrated similarly to pGEX-4T-2 (FIG 16, lane 2) which was expected due to the size of N285, 24 nt (FIG 16, lane 3). pGEX-4T-2/E438 migrated approximately 4.5 kb which ran high than expected, with E438 only being 20 nt in size (FIG 16, lane 4). pGEX-4T-2/Q444 ran similarly to that of pGEX-4T-2/E254 and pGEX-4T-2/N285, migrating approximately 4.1 kb, with Q444 size being 19 nt (FIG 16, lane 5). Differences between the migrations of each ENaC ligand in pGEX-4T-2 compared to the actual size are due to the plasmid DNAs conformations, seen in a supercoiled form as opposed to a linear form or nicked open circular form, which migrate at slower rates due to its topology and hydrodynamic radius. The results from gel electrophoresis correlated precisely with previous results (40).

Expression of GST- ENaC subunit peptides

Previously isolated ENaC ligand plasmids, pGEX-4T-2/E254, pGEX-4T-2/N285, pGEX-4T-2/E438, and pGEX-4T-2/Q444, were retransformed into BL21 (DE3) pLysS cells and were expressed in *E. coli* independently to confirm protein production. Each sample was grown for 3 hours in 2X-YTG media followed by the addition of IPTG, final concentration 100 μ M, and incubated for an additional 3 hours for protein expression.

Cells were centrifuged, removing the supernatant, and lysed by multiple freeze/thaw/cycles. The cell lysates were quantitated via a BCA assay and equal amounts of protein were run on 10% SDS-PAGE gel, through vertical gel electrophoresis, to ensure protein production (FIG 17). GST has an approximate molecular weight of 26 kDa and is fused with the ENaC peptides to utilize in purification, giving the fusion peptide an approximate molecular weight of 29 kDa. GST-N285 migrated approximately 28 kDa with a light background intensity of additional cellular proteins (FIG 17, lane 2). GST-E254 migrated approximately 28 kDa with a heavy background intensity of additional cellular proteins (FIG 17, lane 3). GST-E438 migrated approximately 28 kDa with a faint background intensity of additional cellular proteins (FIG 17, lane 4). GST-Q444 migrated approximately 30 kDa with a very faint background of additional cellular proteins (FIG 17, lane 5). The GST fusion peptides N285, E254, and Q444 expressed well, giving an intense band at the 28 kDa, and E438 was not apparent at this mark. A second band was noticed at approximately 30 kDa in Figure 17 (lanes 2-5) most likely due to the GST fusion protein interaction with cellular proteins, creating an increased shift in migration. GST-E438 does not contain the 26 kDa band in Figure 17 (lane 4) due to low cell lysate concentrations, indicating poor expression levels.

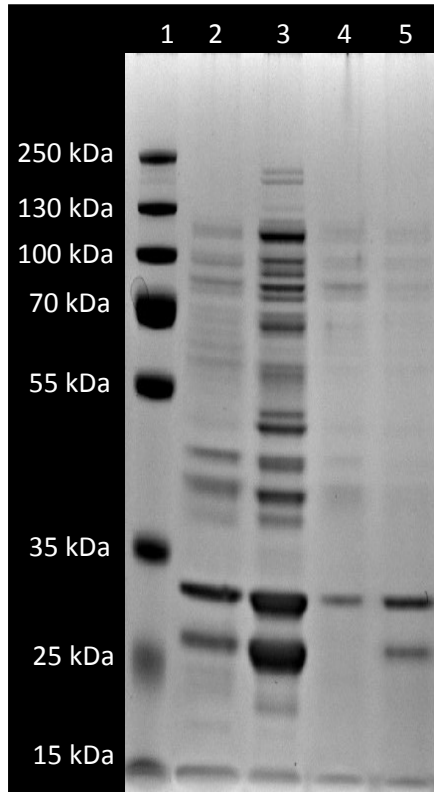


FIG 17. Expressed GST-ENaC fusion proteins in total cell lysates. GST-ENaC ligands were over expressed and run on a 10% SDS-PAGE. Total protein of each sample was 10 μ g. *lane 1*, PageRuler™ Plus Prestained protein ladder. *lane 2*, GST-N285. *lane 3*, GST-E254. *lane 4*, GST-E438. *lane 5*, GST-Q444. The gel was stained with SimplyBlue™ SafeStain.

Purification of GST-fusion peptides

GST fusion peptides that were previously induced were dialyzed and purified via immobilized substrate affinity chromatography (ISAC). The dialysate was incubated with glutathione resin prior to passing through a column to allow for the GST portion of the fusion peptide to interact with the glutathione resin, the substrate for GST.

GST-N285 was noticed in the flow through, running approximately 32 kDa, indicating not all of the fusion protein was captured by the glutathione column (FIG 18, lane 2). The bound GST-N285 was washed with 1X PBS, pH 7.4, further removing any

weakly bound proteins interaction with the glutathione resin (FIG 18, lane 3). Bound GST-N285 was eluted with 10 mM reduced glutathione in 50 mM Tris-HCl, pH 7.4 (FIG 18, lanes 5-7). GST-N285 ran at a single intense band approximately 28 kDa seen in Figure 18 (lanes 5-7), indicating precise purification. The flow through still contained a portion of GST-N285 seen in Figure 18 (lane 2) and can be contributed to high cell lysate concentration to glutathione resin ratio. There is no presence of proteins in the wash see in Figure 18 (lane 3) indicating GST-N285 was strongly interacting with the glutathione resin. GST-N285 was eluted throughout all fractions collected (Fig 18, lanes 5-7) and quantitated via a BCA assay prior to being used for SPR. This resulted in fraction 1 having a total protein content of 427 μg , fraction 2 having a total protein content of 679 μg and fraction 3 having a total protein content of 206 μg (Fig 18, lane 5-7), respectively.

GST-E254 was noticed in the flow through, running approximately 32 kDa, indicating not all of the fusion protein was captured by the glutathione column (FIG 19, lane 2). The bound GST-E254 was washed with 1X PBS, pH 7.4, further removing any weakly bound proteins interaction with the glutathione resin (FIG 19, lane 3). Bound GST-E254 was eluted with 10 mM reduced glutathione in 50 mM Tris-HCl, pH 7.4 (FIG 19, lanes 4-6). GST-E254 ran at a single intense band approximately 28 kDa seen in Figure 19 (lanes 4-6), indicating precise purification. The flow through still contained a portion of GST-E254 seen in Figure 19 (lane 1) and can be contributed to high cell lysate concentration to glutathione resin ratio. There is a high presence of proteins in the wash see in Figure 19 (lane 2) indicating GST-E254 was not intensely interacting with the

glutathione resin. GST-E254 was eluted throughout all fractions collected (Fig 19, lanes 4-6) and quantitated via a BCA assay prior to being used for SPR. This resulted in fraction 1 having a total protein content of 929 μg , fraction 2 having a total protein content of 1.12 mg and fraction 3 having a total protein content of 662 μg (Fig 19, lane 4-6), respectively.

GST-E438 was noticed in the flow through, running approximately 32 kDa, indicating not all of the fusion protein was captured by the glutathione column (FIG 20, lane 2). The bound GST-E438 was washed with 1X PBS, pH 7.4, further removing any weakly bound proteins interaction with the glutathione resin (FIG 20, lane 3). Bound GST-E438 was eluted with 10 mM reduced glutathione in 50 mM Tris-HCl, pH 7.4 (FIG 20, lanes 4-6). GST-E438 ran at approximately 28 kDa as well as higher molecular weights seen in Figure 20 (lanes 4-6), indicating dimerization. The flow through still contained a portion of GST-E438 seen in Figure 20 (lane 2) and can be contributed to high cell lysate concentration to glutathione resin ratio. There is a presence of proteins in the wash see in Figure 20 (lane 3) indicating GST-E438 was not intensely interacting with the glutathione resin. GST-E438 was eluted throughout all fractions collected, though very weak, (FIG 20, lanes 4-6) and quantitated via a BCA assay prior to being used for SPR. This resulted in fraction 1 having a total protein content of 1.31 mg, fraction 2 having a total protein content of 1.28 mg and fraction 3 having a total protein content of 914 μg (FIG 20, lane 4-6), respectively.

GST-Q444 was noticed in the flow through, running approximately 32 kDa, indicating not all of the fusion protein was captured by the glutathione column (FIG 21,

lane 2). The bound GST-Q444 was washed with 1X PBS, pH 7.4, further removing any weakly bound proteins interaction with the glutathione resin (FIG 21, lane 3). Bound GST-Q444 was eluted with 10 mM reduced glutathione in 50 mM Tris-HCl, pH 7.4 (FIG 21, lanes 4-6). GST-Q444 ran at a single intense band approximately 28 kDa (FIG 21, lanes 4-6). The flow through still contained a portion of GST-Q444 seen in Figure 21 (lane 2) and can be contributed to high cell lysate concentration to glutathione resin ratio. There is no presence of proteins in the wash (FIG 21, lane 3) indicating GST-Q444 was strongly interacting with the glutathione resin. GST-Q444 was eluted throughout all fractions collected (FIG 21, lanes 4-6) and quantitated via a BCA assay prior to being used for SPR. This resulted in fraction 1 having a total protein content of 269 μg , fraction 2 having a total protein content of 374 μg and fraction 3 having a total protein content of 227 μg (FIG 21, lane 4-6), respectively.

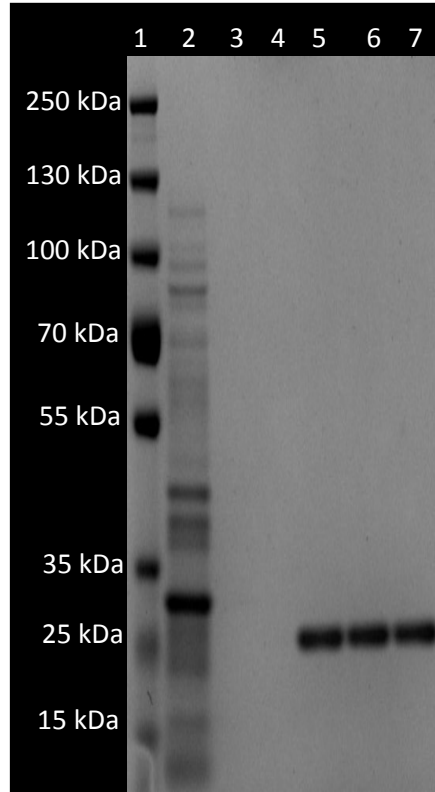


FIG 18. ISAC purification of GST-N285 analyzed by SDS-PAGE. pGEX-4T-2/N285 was transformed into BL21 (DE3) pLysS *E. coli* cells and purified via a glutathione affinity column. Total protein of each sample was 10 μ g. *lane 1*, PageRuler™ Plus Prestained protein ladder. *lane 2*, Cell lysate flow through. *lane 3*, Glutathione column wash. *lane 4*, blank. *lane 5*, fraction 1 of GST-N285. *lane 6*, fraction 2 of GST-N285. *lane 7*, fraction 3 of GST-N285. The gel was stained with SimplyBlue™ SafeStain.

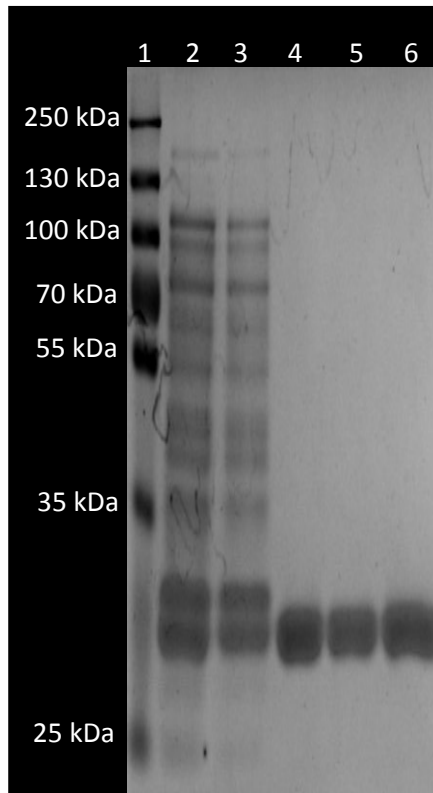


FIG 19. ISAC purification of GST-E254 analyzed by SDS-PAGE. pGEX-4T-2/E254 was transformed into BL21 (DE3) pLysS *E. coli* cells and purified via a glutathione affinity column. Total protein of each sample was 10 μ g. *lane 1*, PageRuler™ Plus Prestained protein ladder. *lane 2*, Cell lysate flow through. *lane 3*, Glutathione column wash. *lane 4*, fraction 1 of GST-E254. *lane 5*, fraction 2 of GST-E254. *lane 6*, fraction 3 of GST-E254. The gel was stained with SimplyBlue™ SafeStain.

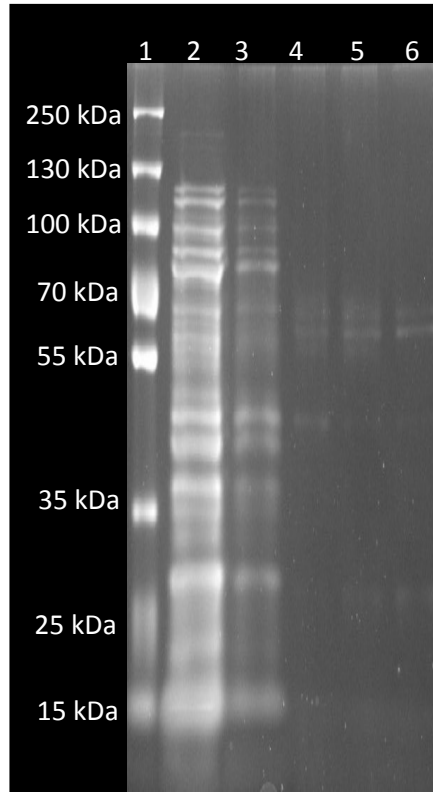


FIG 20. ISAC purification of GST-E438 analyzed by SDS-PAGE. pGEX-4T-2/E438 was transformed into BL21 (DE3) pLysS *E. coli* cells and purified via a glutathione affinity column. Total protein of each sample was 10 μg . *lane 1*, PageRuler™ Plus Prestained protein ladder. *lane 2*, Cell lysate flow through. *lane 3*, Glutathione column wash. *lane 4*, fraction 1 of GST-E438. *lane 5*, fraction 2 of GST-E438. *Lane 6*, fraction 3 of GST-E438. The gel was stained with SimplyBlue™ SafeStain and the image was inverted.

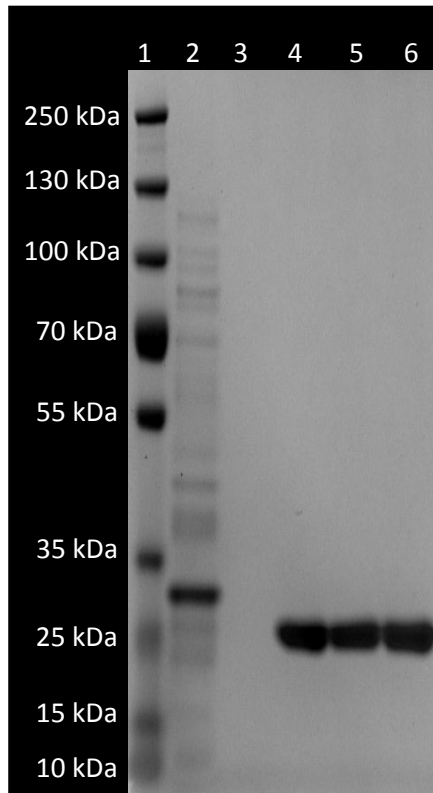


FIG 21. ISAC purification of GST-Q444 analyzed by SDS-PAGE. pGEX-4T-2/Q444 was transformed into BL21 (DE3) pLysS *E. coli* cells and purified via a glutathione affinity column. Total protein of each sample was 10 μ g. *lane 1*, PageRuler™ Plus Prestained protein ladder. *lane 2*, Cell lysate flow through. *lane 3*, Glutathione column wash. *lane 4*, fraction 1 of GST-Q444. *lane 5*, fraction 2 of GST-Q444. *lane 6*, fraction 3 of GST-Q444. The gel was stained with SimplyBlue™ SafeStain.

Thrombin Cleavage of GST-peptides

Prior to GST being cleaved from the ENaC peptides, each peptide was pooled together, respectively, and dialyzed overnight. Pooled GST fusion peptides were agitated with regenerated glutathione resin prior to the addition of thrombin and incubated overnight. The cleaved ENaC peptides were eluted with 1X PBS and collected in one fraction per each peptide and then subjected to a *p*-AminoBenzamidine resin column, to remove thrombin from ENaC peptides. This mixture shook overnight and the ENaC peptides were eluted the following day with 0.4 M NaCl in 50 mM Tris-HCl, pH 8.5. The fractions were collected and quantitated via an extinction coefficient equation as well as a peptide digest assay kit prior to using for SPR (Table 5).

Table 5. Summary of ENaC peptide Fractions quantitated.

Peptide Fraction	$\mu\text{g/mL}$
Q444 F1	180.12
Q444 F2	186.22
E254 F1	666.89
E254 F2	476.35
E438 F1	485.43
E438 F2	355.77
N285 F1	1275.90
N285 F2	1344.45

C. SPR Analysis

CM5 Chip Activation

After the CM5 chip was activated, anti-GST was immobilized onto the chip through amine coupling. Anti-GST was bound to both flow cells, 1 and 2, to analyze and reference the kinetic interactions (FIG 22 A). Recombinant GST was ran over both flow cells to block high affinity binding sites to prevent inaccurate readings during binding assays. An increase in response units was observed on both flow cells indicating the recombinant GST bound. The immobilization captured approximately 5000 pg on flow cell 1 and 5000 pg on flow cell 2. Regeneration solution was added to flow cell 1 to remove recombinant GST from anti-GST, for binding of GST fusion peptides, and flow cell 2 was left untouched to server as a reference cell (FIG 22 A). Immediately after flow cell 1 was regenerated, GST fusion peptide E438 was immobilized to anti-GST by two injections at a concentration of 200 mg/mL with a response change of 200 RU, 200 pg of material (FIG 22 B). This can be seen more clearly in Figure 22 (C-D) elucidating unbound fusion peptide and immobilization of fusion peptide, respectively. Each fusion peptide was bound under these same conditions with regeneration solution used to completely unbind each fusion peptide to add the next one. Also, when whole α ENaC subunits were run over each GST fusion peptide, lower concentrations had to be used due to high buffer shift effects since α ENaC and α His2- α ENaC were purified and isolated in a weak ionic/non-ionic buffer. α ENaC here is used as a control to ensure that the 6X histidine tag of α His2- α ENaC is not responsible for the interaction with the peptide.

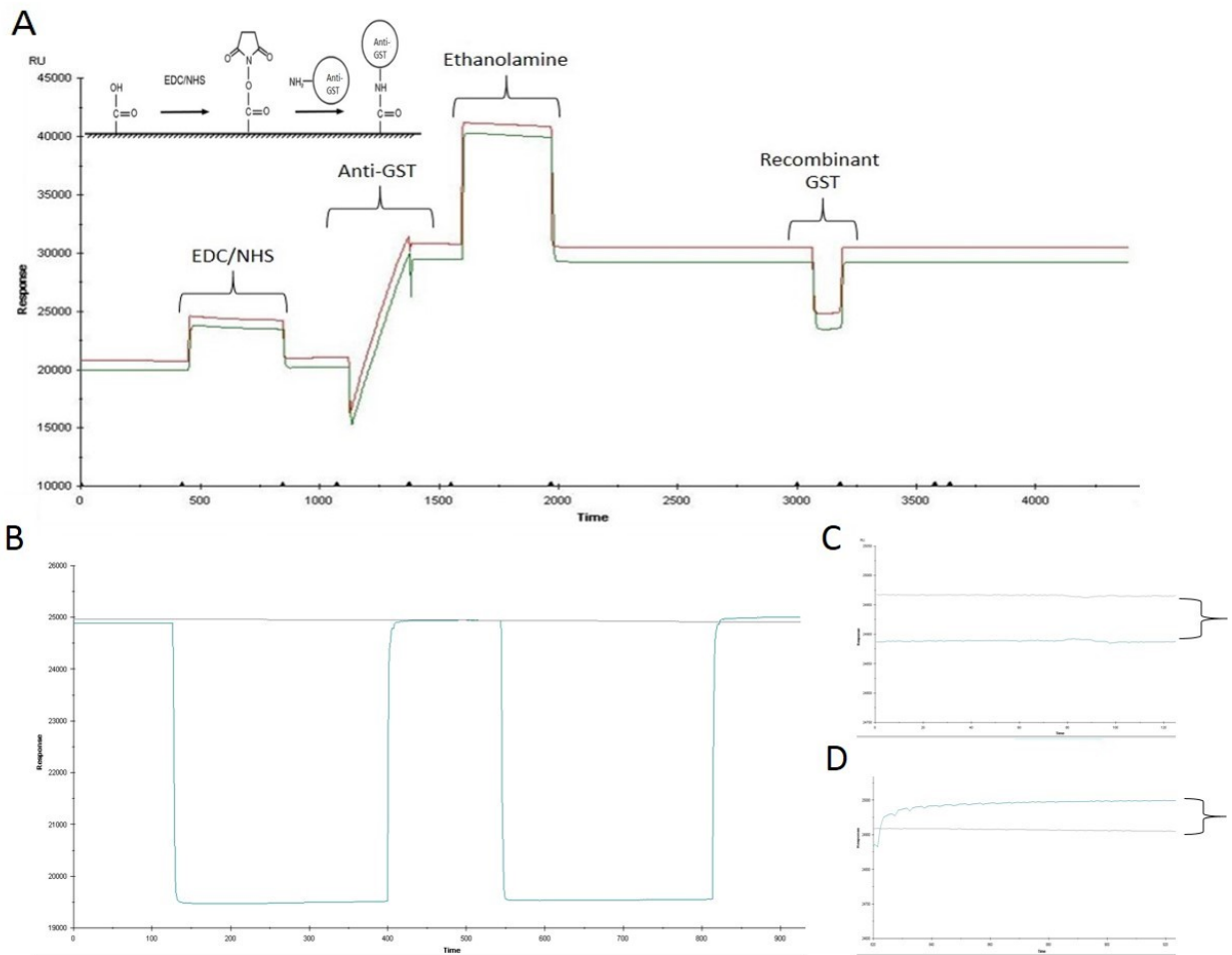


FIG 22. CM5 chip activation and Immobilization of GST-E438. A CM5 sensor chip was activated and anti-GST was bound to capture GST fusion peptides. **A** – Stepwise activation of CM5 chip, flow cell 1 (red) and flow cell 2 (green). **B** – Immobilization of GST-E438 to anti-GST, flow cell 1 (blue) and flow cell 2 (grey). **C** – Unbound response of GST fusion peptides at time 0 - 100 sec, flow cell 1 (blue) and flow cell 2 (grey). **D** – Immobilization of GST E438 to anti-GST at time 815 – 915 sec, flow cell 1 (blue) and flow cell 2 (grey).

GST-fusion peptide binding assays - GST-E438 (β -thumb) vs N285 (α -palm)

The binding assay was conducted using increasing analyte N285 concentrations at 90, 150, 250, and 350 $\mu\text{g}/\text{mL}$, with a 60 μL injection volume at 5 $\mu\text{L}/\text{min}$ (FIG 23). The binding data was analyzed using BIAevaluation software to retrieve the kinetic data (FIG 23). An association constant of $3.35 \times 10^8 \text{ M}^{-1}$ and a dissociation constant of $2.99 \times 10^{-9} \text{ M}$ was determined, with a χ^2 of 3.34 (Table 6). The results support a reproducible association although not strong, it is noticeable, and is within the range of a non-covalent interaction. This could be due to each of these peptides being part of a larger binding event which would be probable since E438 is part of αENaC , palm region, and N285 is part of βENaC , thumb region.

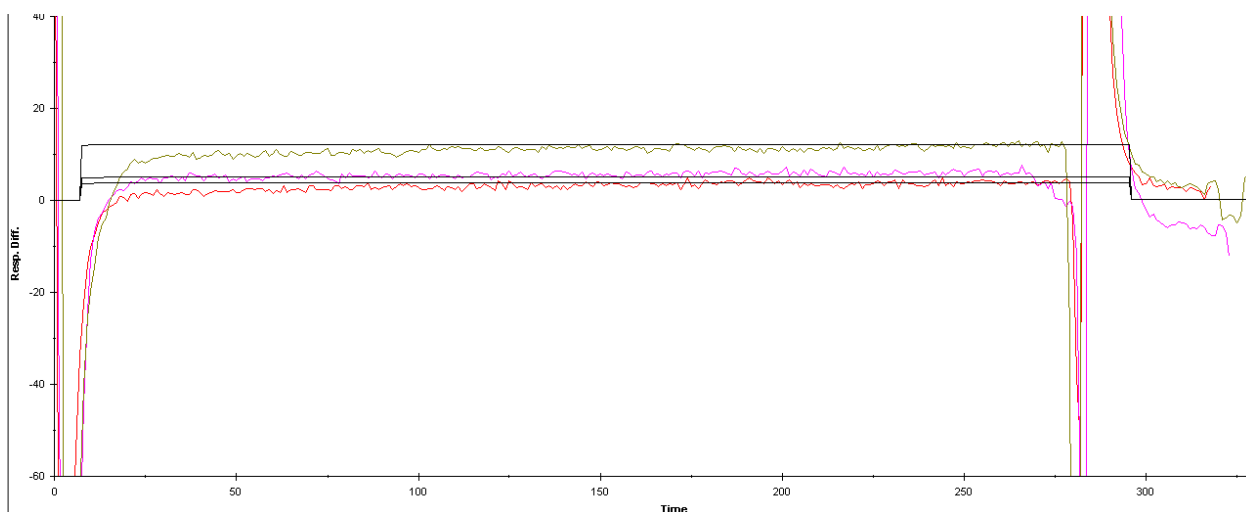


FIG 23. Kinetic evaluation of binding assay of N285 analyte to GST fusion peptide E438. Increasing analyte concentrations of N285 binding to GST-E438 fusion peptide with concentrations of 90 $\mu\text{g}/\text{mL}$ (red), 150 $\mu\text{g}/\text{mL}$ (violet), and 250 $\mu\text{g}/\text{mL}$ (gold). Samples were run with 60 μL injections at 5 $\mu\text{L}/\text{min}$, $n = 3$.

Table 6. GST-E438 vs N285 kinetics. Kinetic values obtained from analyte N285 interactions with GST fusion peptide E438 via BIAevaluation.

K_{on} (1/ Ms)	K_{off} (1/s)	K_A (1/ M)	K_D (M)	χ^2
6.82×10^3	2.04×10^{-5}	3.35×10^8	2.99×10^{-9}	3.34

GST-fusion peptide binding assays - GST-N285 (α -palm) vs E438 (β -thumb)

The reverse binding assay was conducted to verify the previous GST fusion peptide and analyte kinetic data. It was run under the same conditions as the previous study (FIG 24). The binding data was analyzed using BIAevaluation software to retrieve the kinetic data (FIG 24). An association constant of $2.48 \times 10^7 \text{ M}^{-1}$ and a dissociation constant of $4.03 \times 10^{-8} \text{ M}$ was determined, with a χ^2 of 2.46 (Table 7). The results correlate with the previous study further verifying that these peptide portions may be part of a larger binding event between the two different subunits and represent a non-covalent interaction.

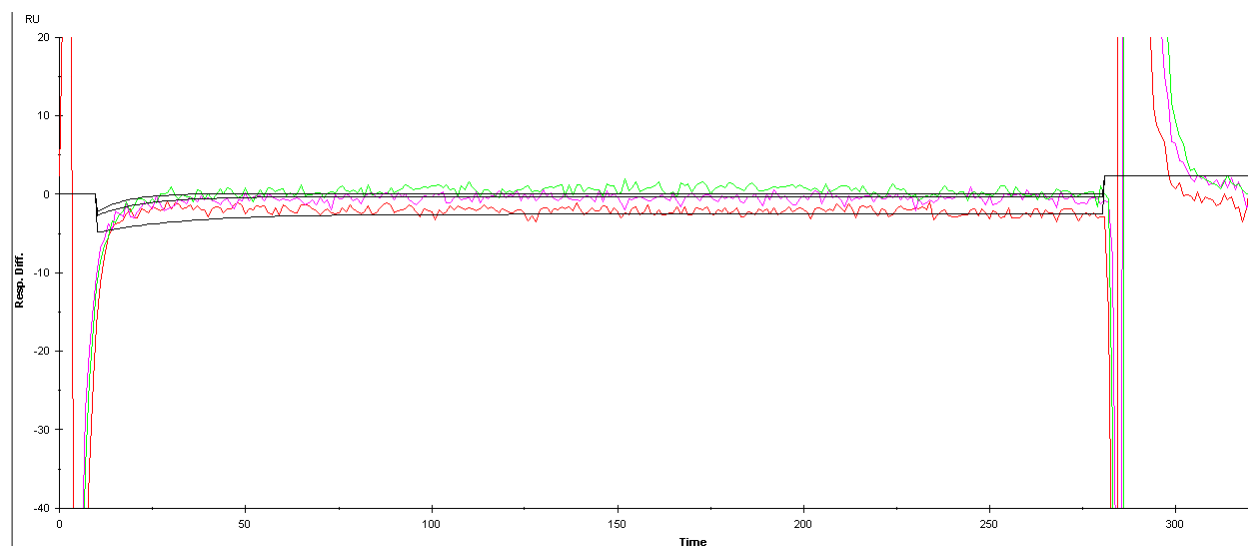


FIG 24. Kinetic evaluation of binding assay of E438 analyte to GST fusion peptide N285. Increasing analyte concentrations of E438 binding to GST-N285 fusion peptide with concentrations of 90 µg/mL (red), 150 µg/mL (violet), and 250 µg/mL (green). Samples were run with 60 µL injections at 5 µL/min, $n = 3$.

Table 7. GST-N285 vs E438 kinetics. Kinetic values obtained from analyte E438 interactions with GST fusion peptide N285 via BIAevaluation.

K_{on} (1/ Ms)	K_{off} (1/s)	K_A (1/ M)	K_D (M)	χ^2
3.01×10^3	1.21×10^{-4}	2.48×10^7	4.03×10^{-8}	2.46

GST-fusion peptide binding assays - GST-E254 (β -palm) vs Q444 (γ -thumb)

The binding assay was conducted using increasing analyte Q444 concentrations at 6, 12, 23, and 46 µg/mL, with a 60 uL injection volume at 5 µL/min (FIG 25). The binding data was analyzed using BIAevaluation software to retrieve the kinetic data (FIG 25). An association constant of $1.66 \times 10^3 \text{ M}^{-1}$ and a dissociation constant of $6.01 \times 10^{-4} \text{ M}$ was determined, with a χ^2 of 3.27 (Table 8). The results demonstrated a slight association pattern however favoring more of a strong dissociation pattern. These

results are much weaker when compared to E438 and N285 and seem as if each of the peptides are a portion of one binding domain whereas the E438 and N285 interaction could itself be a binding domain.

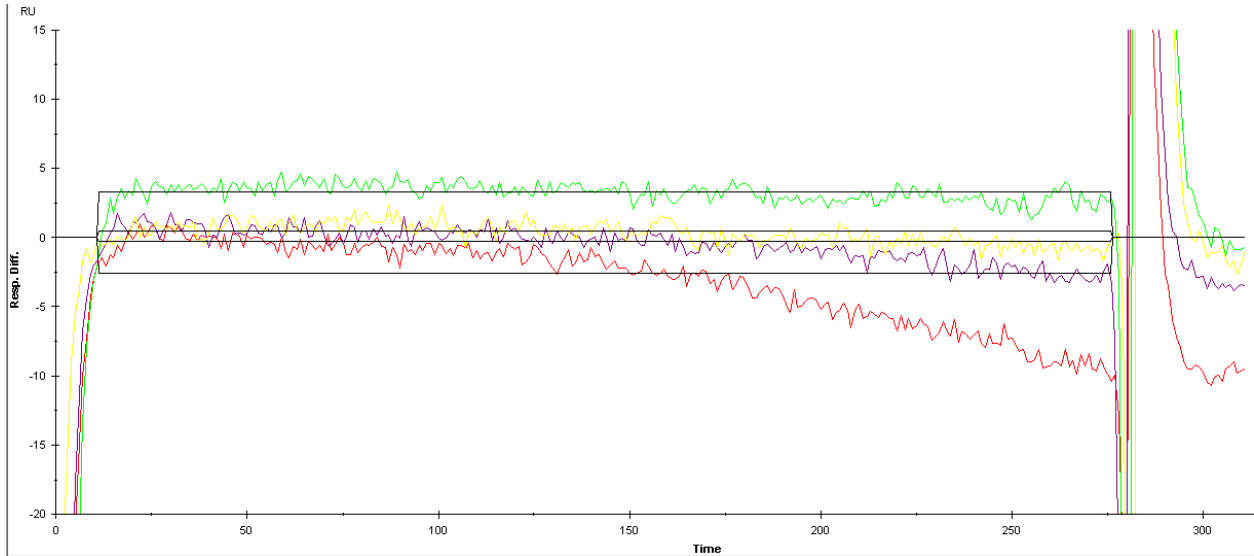


FIG 25. Kinetic evaluation of binding assay of Q444 analyte to GST fusion peptide E254. Increasing analyte concentrations of Q444 binding to GST-E254 fusion peptide with concentrations of 6 µg/mL (red), 12 µg/mL (purple), 23 µg/mL (yellow), and 46 µg/mL (green). Samples were run with 60 µL injections at 5 µL/min, $n = 3$.

Table 8. GST-E254 vs Q444 kinetics. Kinetic values obtained from analyte Q444 interactions with GST fusion peptide E254 via BIAevaluation.

K_{on} (1/ Ms)	K_{off} (1/s)	K_A (1/ M)	K_D (M)	χ^2
0.151	9.09×10^{-5}	1.66×10^3	6.01×10^{-4}	3.27

GST-fusion peptide binding assays - GST-Q444 (γ -thumb) vs E254 (β -palm)

The reverse binding assay was conducted to verify the previous GST fusion peptide and analyte kinetic data. It was run under the same conditions as the previous study, with the exception of 46 $\mu\text{g}/\text{mL}$ of analyte exempted due to buffer shifting errors (FIG 26). The binding data was analyzed using BIAevaluation software to retrieve the kinetic data (FIG 26). An association constant of $2.12 \times 10^5 \text{ M}^{-1}$ and a dissociation constant of $4.71 \times 10^{-6} \text{ M}$ was determined, with a χ^2 of 6.92 (Table 9). The results do not correlate to the previous experiment, showing a difference of 4 orders of magnitude in K_D . This could be due to a difference in secondary structure when the peptide is free versus when it is fused with GST.

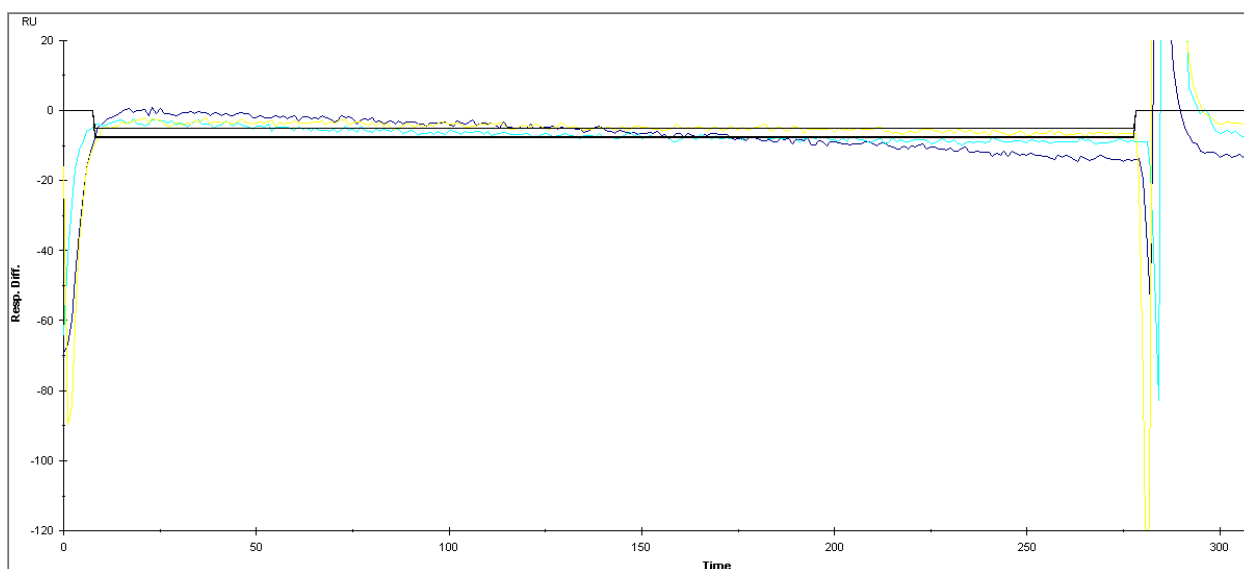


FIG 26. Kinetic evaluation of binding assay of E254 analyte to GST fusion peptide Q444. Increasing analyte concentrations of E254 binding to GST-Q444 fusion peptide with concentrations of 6 $\mu\text{g}/\text{mL}$ (cyan), 12 $\mu\text{g}/\text{mL}$ (yellow), and 23 $\mu\text{g}/\text{mL}$ (blue) Samples were run with 60 μL injections at 5 $\mu\text{L}/\text{min}$, $n = 3$.

Table 9. GST-Q444 vs E254 kinetics. Kinetic values obtained from analyte E254 interactions with GST fusion peptide Q444 via BIAevaluation.

K_{on} (1/ Ms)	K_{off} (1/s)	K_A (1/ M)	K_D (M)	χ^2
2.14	1.01×10^{-5}	2.12×10^5	4.71×10^{-6}	6.92

GST-fusion peptide binding assays - GST-E438 (β -thumb) vs α ENaC

The binding assay was conducted using increasing analyte α ENaC concentrations at 1.25, 2.5, 5, and 10 μ g/mL, with a 60 μ L injection volume at 5 μ L/min (FIG 27). The binding data was analyzed using BIAevaluation software to retrieve the kinetic data (FIG 27). An association constant of $7.91 \times 10^7 \text{ M}^{-1}$ and a dissociation constant of $1.26 \times 10^{-8} \text{ M}$ was determined, with a χ^2 of 0.349 (Table 10). The results support a reproducible association although not strong, it is noticeable, and is within the range of a non-covalent interaction. This is similar to the interaction noticed between E438 and N2854 where this interaction too could be associated with a larger binding event.

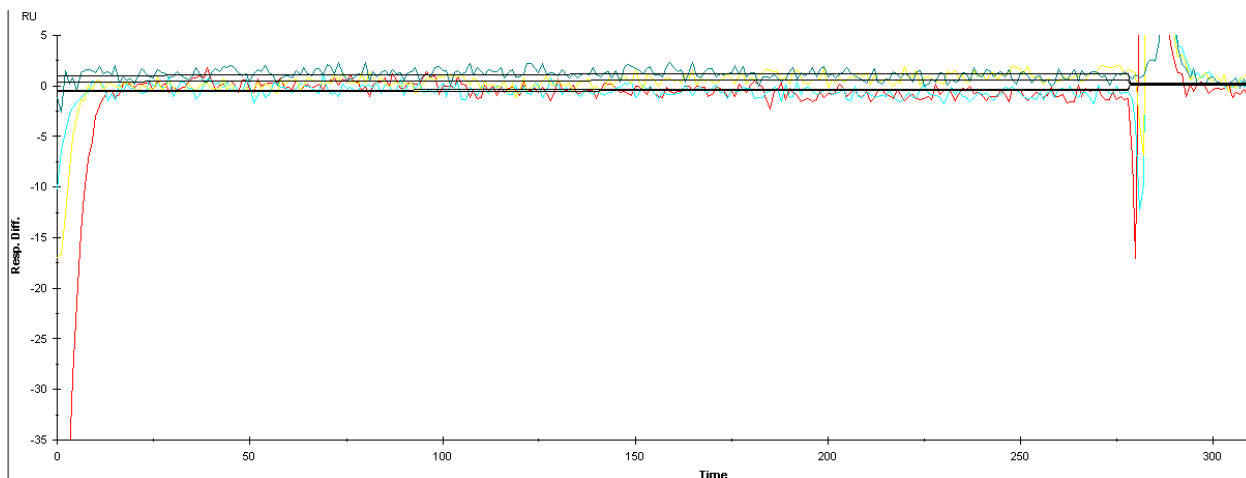


FIG 27. Kinetic evaluation of binding assay of α ENaC analyte to GST fusion peptide E438. Increasing analyte concentrations of α ENaC binding to GST-E438 fusion peptide with concentrations of 1.25 $\mu\text{g}/\text{mL}$ (red), 2.5 $\mu\text{g}/\text{mL}$ (cyan), 5 $\mu\text{g}/\text{mL}$ (yellow), and 10 $\mu\text{g}/\text{mL}$ (blue). Samples were run with 60 μL injections at 5 $\mu\text{L}/\text{min}$, $n = 3$.

Table 10. GST-E438 vs α ENaC kinetics. Kinetic values obtained from analyte α ENaC interactions with GST fusion peptide E438 via BIAevaluation.

K_{on} (1/ Ms)	K_{off} (1/s)	K_{A} (1/ M)	K_{D} (M)	Chi^2
3.19×10^3	4.04×10^{-5}	7.91×10^7	1.26×10^{-8}	0.349

GST-fusion peptide binding assays - GST-N285 (α -palm) vs α ENaC

The binding assay was conducted under the same conditions as the previous one (FIG 28). The binding data was analyzed using BIAevaluation software to retrieve the kinetic data (FIG 28). An association constant of $1.3 \times 10^8 \text{ M}^{-1}$ and a dissociation constant of $7.67 \times 10^{-9} \text{ M}$ was determined, with a chi^2 of 0.349 (Table 11). The results support a reproducible association although not strong, it is noticeable, is within the range of a non-covalent interaction. This data shows that this interaction was stronger than E438

which is interesting because we would expect α ENaC to interact better with another subunit versus itself.

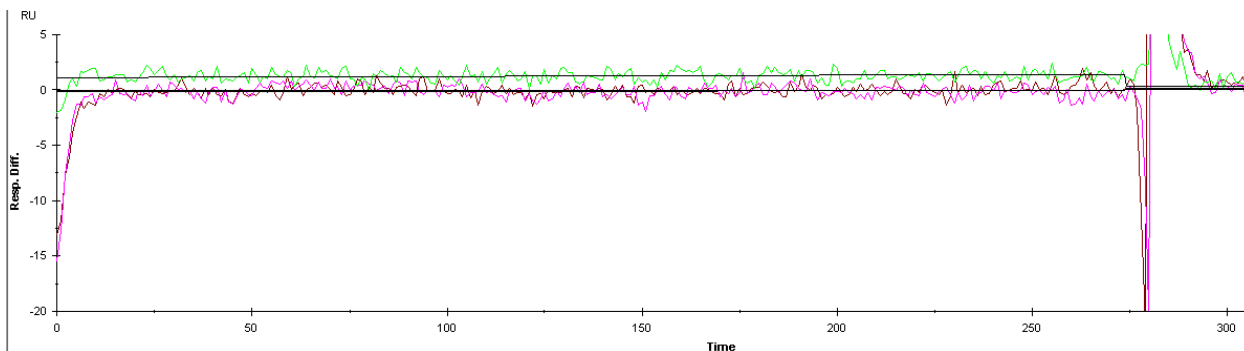


FIG 28. Kinetic evaluation of binding assay of α ENaC analyte to GST fusion peptide N285. Increasing analyte concentrations of α ENaC binding to GST-N285 fusion peptide with concentrations of 1.25 $\mu\text{g/mL}$ (maroon), 2.5 $\mu\text{g/mL}$ (purple), and 5 $\mu\text{g/mL}$ (green). Samples were run with 60 μL injections at 5 $\mu\text{L/min}$, $n = 3$.

Table 11. GST-N285 vs α ENaC kinetics. Kinetic values obtained from analyte α ENaC interactions with GST fusion peptide N285 via BIAevaluation.

K_{on} (1/ Ms)	K_{off} (1/s)	K_{A} (1/ M)	K_{D} (M)	Chi^2
1.43×10^3	1.1×10^{-5}	1.3×10^8	7.67×10^{-9}	0.283

GST-fusion peptide binding assays - GST-E254 (β -palm) vs α ENaC

The binding assay was conducted under the same conditions as the previous one (FIG 29). The binding data was analyzed using BIAevaluation software to retrieve the kinetic data (FIG 29). An association constant of $1.34 \times 10^4 \text{ M}^{-1}$ and a dissociation constant of $7.48 \times 10^{-5} \text{ M}$ was determined, with a chi^2 of 0.816 (Table 12). The results

support a very weak association and is similar to the results from the interaction of E254 vs Q444, where this peptide partially interacted with α ENaC and would most likely be a portion of one binding domain, not the full domain.

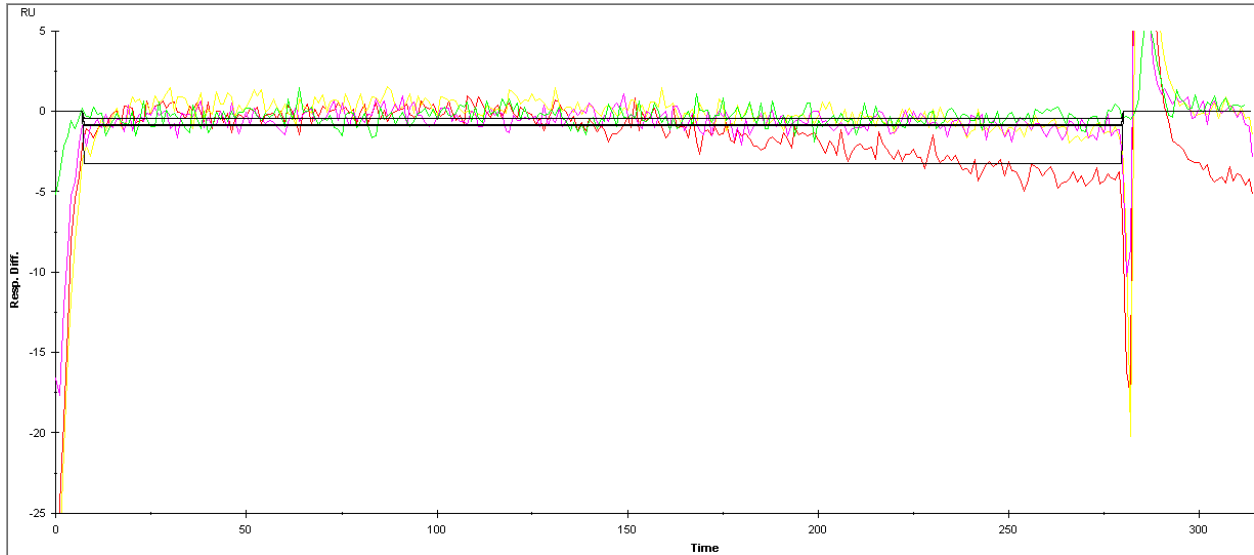


FIG 29. Kinetic evaluation of binding assay of α ENaC analyte to GST fusion peptide E254. Increasing analyte concentrations of α ENaC binding to GST-E254 fusion peptide with concentrations of 1.25 $\mu\text{g/mL}$ (red), 2.5 $\mu\text{g/mL}$ (violet), 5 $\mu\text{g/mL}$ (yellow), and 10 $\mu\text{g/mL}$ (green). Samples were run with 60 μL injections at 5 $\mu\text{L/min}$, $n = 3$.

Table 12. GST-E254 vs α ENaC kinetics. Kinetic values obtained from analyte α ENaC interactions with GST fusion peptide E254 via BIAevaluation.

K_{on} (1/ Ms)	K_{off} (1/s)	K_{A} (1/ M)	K_{D} (M)	Chi^2
0.134	1×10^{-5}	1.34×10^4	7.67×10^{-5}	0.816

GST-fusion peptide binding assays - GST-E438 (β -thumb) vs α His2- α ENaC

The binding assay was conducted using increasing analyte α His2- α ENaC concentrations at 1.25, 2.5, and 5 μ g/mL, with a 60 μ L injection volume at 5 μ L/min (FIG 30). The binding data was analyzed using BIAevaluation software to retrieve the kinetic data (FIG 30). An association constant of $2.1 \times 10^7 \text{ M}^{-1}$ and a dissociation constant of $4.77 \times 10^{-8} \text{ M}$ was determined, with a χ^2 of 0.286 (Table 13). The results support a reproducible association although not strong, it is noticeable, and is within the range of a non-covalent interaction. This is similar to the interaction noticed between E438 and N2854 where this interaction could be associated with a larger binding event.

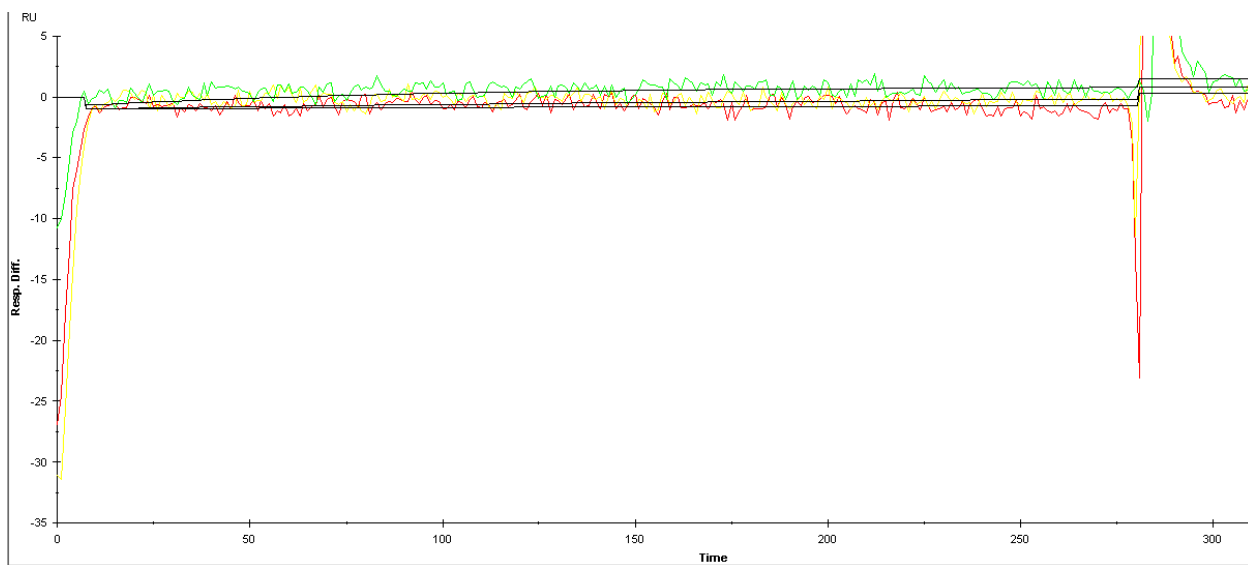


FIG 30. Kinetic evaluation of binding assay of α His2- α ENaC analyte to GST fusion peptide E438.

Increasing analyte concentrations of α His2- α ENaC binding to GST-E438 fusion peptide with concentrations of 1.25 μ g/mL (red), 2.5 μ g/mL (yellow), and 5 μ g/mL (green). Samples were run with 60 μ L injections at 5 μ L/min, $n = 3$.

Table 13. GST-E438 vs α His2- α ENaC kinetics. Kinetic values obtained from analyte α His2- α ENaC interactions with GST fusion peptide E438 via BIAevaluation.

K_{on} (1/ Ms)	K_{off} (1/s)	K_A (1/ M)	K_D (M)	χ^2
2.51×10^3	1×10^{-4}	2.1×10^7	4.77×10^{-8}	0.286

GST-fusion peptide binding assays - GST-N285 (α -palm) vs α His2- α ENaC

The binding assay was conducted using increasing analyte α His2- α ENaC concentrations at 1.25, 2.5, and 5 μ g/mL, with a 60 μ L injection volume at 5 μ L/min (FIG 31). The binding data was analyzed using BIAevaluation software to retrieve the kinetic data (FIG 31). An association constant of $1.44 \times 10^{10} \text{ M}^{-1}$ and a dissociation constant of $6.94 \times 10^{-11} \text{ M}$ was determined, with a χ^2 of 0.294 (Table 14). The results support a reproducible association although not strong, it is noticeable, and is within the range of a non-covalent interaction. This is similar to the interaction noticed between E438 and N2854 where this interaction could be associated with a larger binding event.

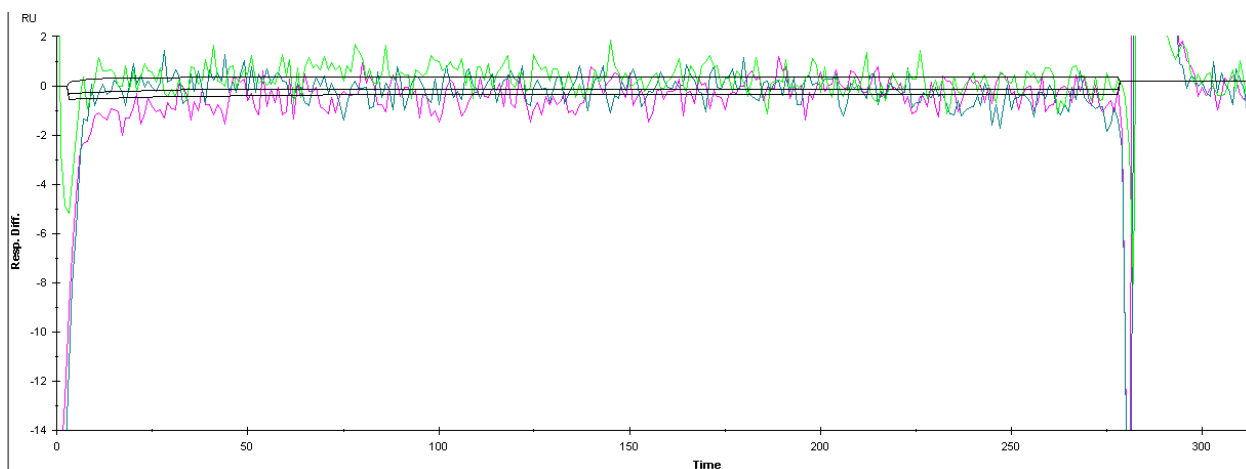


FIG 31. Kinetic evaluation of binding assay of α His2- α ENaC analyte to GST fusion peptide N285.

Increasing analyte concentrations of α His2- α ENaC binding to GST-N285 fusion peptide with concentrations of 1.25 μ g/mL (purple), 2.5 μ g/mL (blue), and 5 μ g/mL (green). Samples were run with 60 μ L injections at 5 μ L/min, $n = 3$.

Table 14. GST-N285 vs α His2- α ENaC kinetics. Kinetic values obtained from analyte α His2- α ENaC interactions with GST fusion peptide N285 via BIAevaluation.

K_{on} (1/ Ms)	K_{off} (1/s)	K_A (1/ M)	K_D (M)	Chi ²
4.63×10^4	3.21×10^{-6}	1.44×10^{10}	6.94×10^{-11}	0.294

GST-fusion peptide binding assays - GST-E254 (β -palm) vs α His2- α ENaC

The binding assay was conducted using increasing analyte α His2- α ENaC concentrations at 1.25, 2.5, and 5 μ g/mL, with a 60 μ L injection volume at 5 μ L/min (FIG 32). The binding data was analyzed using BIAevaluation software to retrieve the kinetic data (FIG 32). An association constant of $1.03 \times 10^5 \text{ M}^{-1}$ and a dissociation constant of $9.7 \times 10^{-6} \text{ M}$ was determined, with a chi² of 0.641 (Table 15). The results support a very weak association and is similar to the results from the interaction of E254 vs Q444,

where this peptide partially interacted with α ENaC and would most likely be a portion of one binding domain, not the full domain.

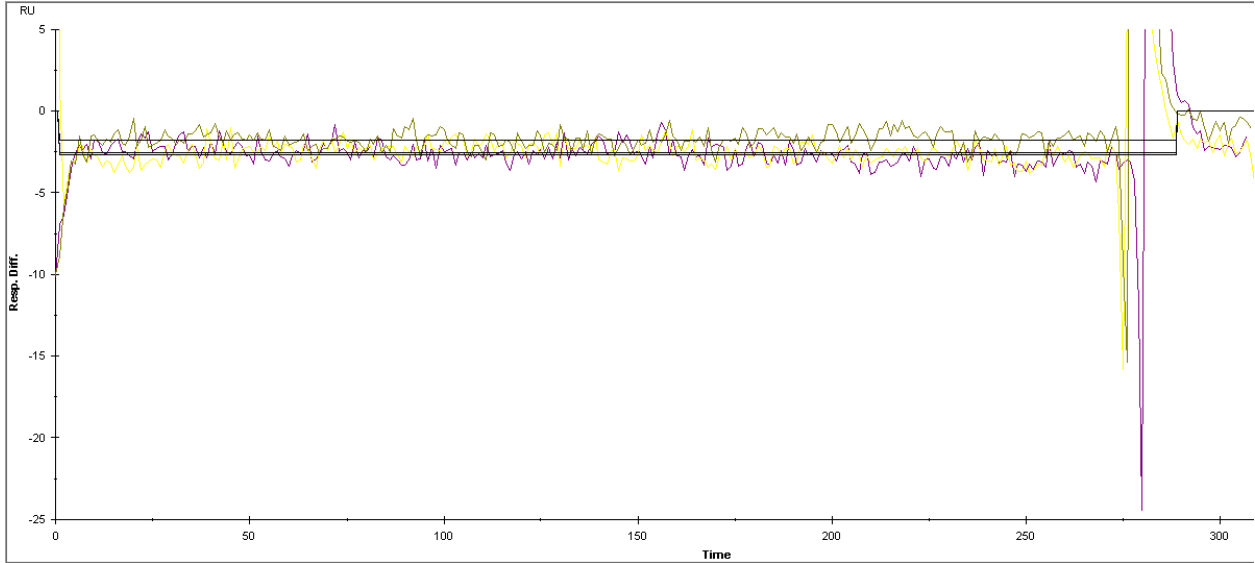


FIG 32. Kinetic evaluation of binding assay of α His2- α ENaC analyte to GST fusion peptide E254.

Increasing analyte concentrations of α His2- α ENaC binding to GST-E254 fusion peptide with concentrations of 1.25 μ g/mL (yellow), 2.5 μ g/mL (violet), and 5 μ g/mL (gold). Samples were run with 60 μ L injections at 5 μ L/min, $n = 3$.

Table 15. GST-E254 vs α His2- α ENaC kinetics. Kinetic values obtained from analyte α His2- α ENaC interactions with GST fusion peptide E254 via BIAevaluation.

K_{on} (1/ Ms)	K_{off} (1/s)	K_A (1/ M)	K_D (M)	χ^2
4.01×10^4	3.89×10^{-5}	1.03×10^5	9.7×10^{-6}	0.641

IV. CONCLUSION

The alpha subunit of the epithelial sodium channel containing a 6X histidine tag (α His2- α ENaC) has been partially purified in this study. It was established that an 8 hr induction time was ideal for maximum protein production and that using acid washed glass beads with RIPA buffer was ideal for protein extraction. The methods employed eliminated non-ENaC proteins and gave μ g concentrations. Do to the total protein of purified α ENaC isolated through immobilize nickel affinity chromatography, studies can now benefit from this purification scheme to perform structural studies.

The peptide portions of ENaC were purified in a vigorous step wise manner through glutathione affinity chromatography and *p*-Benzamidine chromatography, allowing them to be subjected to SPR.

Interactions between immobilized E438 (β -thumb) and peptide N285 (α -palm) showed an associative binding interaction when compared to the reference flow cell. The kinetic evaluation of this interaction presenting kinetic constants in the range of non-covalent interactions, this was also true for the reverse interaction (FIG 23, 24). Interactions between immobilized E254 (β -palm) and peptide Q444 (γ -thumb) also showed an associative binding interaction however much weaker than the previous reaction, this was also true for the reverse interaction (FIG 25, 26).

Interactions between immobilized E254 (β -palm) with α ENaC and α His- α ENaC, separately, showed a weak association interaction action similar to that between E254 (β -palm) and Q444 (γ -thumb) seen in Figure 29 and 32. Interactions between

immobilized E438 (β -thumb) with α ENaC and α His- α ENaC, separately, showed a strong associative binding interaction giving kinetic constants in the non-covalent range, also seen above with E438 (β -thumb) and peptide N285 (α -palm) seen in Figure 27 and 30. This was also seen in the interaction between immobilized N285 with α ENaC and α His- α ENaC, separately (FIG 28, 31).

The results of this study prove a purification scheme to isolate native α ENaC as well as modified ENaCs with extracellular loop histidine tags. They show associated kinetic interactions in the range of non-covalent interactions between the β -thumb region of β ENaC and the α -palm region of α ENaC (Table 16). Due to high buffer shifts, immobilized Q444 could not be assayed with α ENaC or α His- α ENaC. Future studies would seek to use longer peptides containing these ENaC subunit regions to elucidate if they are part of a larger binding event for the formation of heterotrimeric ENaC in structural studies.

Table 16. Summary of Kinetics. Kinetic values were obtained from BIAevaluation software. This table summarizes the binding affinities identified from individual binding assays. * Grant Peltier's average K_D values. ** Chance Berman's average K_D values.

Interaction description	Peptide Interaction	K_D (1/M)*	K_D (M)**	SEM
β -thumb to α -palm	GST-E438 to N285	2.88×10^{-8}	4.87×10^{-9}	$1.68 \times 10^{-8} \pm 1.69 \times 10^{-8}$
α -palm to β -thumb	GST-N285 to E438	N/A	3.18×10^{-9}	$3.18 \times 10^{-9} \pm 8.5 \times 10^{-10}$
β -palm to γ -thumb	GST-E254 to Q444	2.76×10^{-5}	3.11×10^{-4}	$1.69 \times 10^{-4} \pm 2.00 \times 10^{-4}$
γ -thumb to β -palm	GST-Q444 to E254	N/A	3.89×10^{-9}	$3.89 \times 10^{-9} \pm 2.73 \times 10^{-9}$
β -thumb to α -subunit	GST-E438 to α ENaC	N/A	2.07×10^{-8}	$2.07 \times 10^{-8} \pm 1.99 \times 10^{-8}$
α -palm to α -subunit	GST-N285 to α ENaC	N/A	7.56×10^{-9}	$7.56 \times 10^{-9} \pm 1.10 \times 10^{-10}$
β -palm to α -subunit	GST-E254 to α ENaC	N/A	2.63×10^{-5}	$2.63 \times 10^{-5} \pm 3.43 \times 10^{-5}$
β -thumb to α -subunit	GST-E438 to α His2- α ENaC	N/A	4.80×10^{-8}	$4.80 \times 10^{-8} \pm 2.41 \times 10^{-8}$
α -palm to α -subunit	GST-N285 to α His2- α ENaC	N/A	2.73×10^{-10}	$2.73 \times 10^{-10} \pm 2.03 \times 10^{-10}$
β -palm to α -subunit	GST-E254 to α His2- α ENaC	N/A	4.24×10^{-6}	$4.24 \times 10^{-6} \pm 3.87 \times 10^{-6}$

LITERATURE CITED

1. Alvarez de la Rosa, D., Navarro-González, J.F., and Giraldez, T. *Curr. Mol. Pharmacol.* **2013**, 6, 35-43.
2. Bhalla, V., and Hallows, K.R. *JASN.* **2008**, 19, 1845-54.
3. <http://www.beltina.org/pics/nephron.jpg>
4. Post, R., Sen, A., and Rosenthal, A. *J. Biol. Chem.* **1965**, 240, 1437-45.
5. Schild, L. *Biochim. Biophys. Acta.* **2010**, 1802, 1159-65.
6. http://www.hkmacme.org/course/2009BM0011-01-00/sp1109_f7.png
7. Giraldez, T., Rojas, P., Jou, J., Flores, C., and Alvarez de la Rosa, D. *Am. J. Physiol.* **2012**, 303, F328-F38.
8. Kellenberger, S. and Schild, L. *Physiol Rev.* **2002**, 82 (3): 735-767.
9. Hangukoglu, I., and Hanukoglu, A. *Gene.* **2016**, 579, 95-132.
10. Kashlan, O.B., et al. *J. Biol. Chem.* **2011**, 286, 649-60.
11. Starushenko, A., Adams, E., Booth, R.E., and Stockand, J.D. **2005**, 88, 3966-75.
12. Hanukoglu, I. *FEBS J.* **2016**, doi: 10.1111/febs.13840.
13. McNicholas, C., and Canessa, C. *J. Gen. Physiol.* **1997**, 109, 681-92.
14. Stockand, J.D., Staruschenko, A., Pochynyuk, O., Booth, R.E., and Silverthorn, D.U. *Life.* **2008**, 60, 620-28.
15. Jasti, J., Furukawa, H., Gonzales, E.B., and Gouaux, E. *Nature.* **2007**, 449, 316 -23.
16. <http://ajprenal.physiology.org/content/ajprenal/301/4/F684/F1.large.jpg>
17. Butterworth, M.B. *Biochim. Biophys. Acta.* **2010**, 1802, 1166-77.
18. Peters, K.W., Qi, J., Johnson, J.P. et al. *Pflügers Arch.-Eur. J. Physiol.* **2001**, 443, S65.
19. Stockand, J.D. *Kidney Int.* **2010**, 78, 849-56.
20. Butterworth, M.B., Edinger, R.S., and Frizzell, R.A. *Am. J. Physiol. Renal Physiol.* **2008**, 296, F10-24.
21. Yu, L., Helms, M.N., Yue, W., and Eaton, D.C. *Am. J. Physiol. Renal. Physiol.* **2008**, 295, F1519-F27.
22. Snyder, P.M., Cheng, C., Prince, L.S., Rodgers, J.C., and Welsh, M.J. *J. Biol. Chem.* **1998**, 273, 681-84.
23. Zhou, R., Patel S.V., and Snyder, P.M. *J. Biol. Chem.* **2007**, 282, 20207-12.
24. Liang, X. et al. *J. Biol. Chem.* **2008**, 283, 27418-25.
25. Staub, O., Gautschi, I., Ciechanover, A., Schild, L, and Rotin, D. *EMBO J.* **1997**, 21, 6325-36.
26. Snyder, P.M. *Endocrine Reviews.* **2002**, 23, 258-75.
27. Oh, Y.S., and Warnock, D.G. *Exp. Nephrol.* **2000**, 8, 320-5.
28. Gründer, S. et al. *EMBO J.* **1997**, 16, 899-907.
29. Zeissg, S. et al. *Am. J. Gastroenterol.* **2008**, 134, 1436-47.
30. Azad, A.K. et al. *Hum. Mutat.* **2009**, 30, 1093-103.
31. Sinha, R., Salphale, I., and Agarwal, I. *Indian. J. Pediatr.* **2013**, 80, 878-80.
32. Hummler, E. et al. *Proc. Natl. Acad. Sci.* **1997**, 94, 11710-15.

33. Bonny, O. *et al. J. Clin. Invest.* **1999**, 104, 967-74.
34. Geller, D.S. *et al. J. Am. Soc. Nephrol.* **2006**, 17, 1429-36.
35. Zeissig, S. *et al. Am. J. Gastroent.* **2008**, 134, 1436-47.
36. Hobbs, C.A., Da Tan, C., and Tarran R. *J. Physiol.* **2013**, 591, 4388-87.
37. Rauh, R. *et al. J. Physiol.* **2010**, 588, 1211-25.
38. Collawn, J.F., Lazark, A., Bebok, Z., and Matalon, S. *Am. J. Physiol. Lung Cell Mol. Physiol.* **2012**, 302, L1141-46.
39. Chung, C.T., and Miller, R.H. *Nucleic Acids Research.* **1988**, 16(8), 3580.
40. Peltier, G.C. **2012**, Determining Critical Residues for Intersubunit Binding of the Human Epithelial Sodium Channel. *M.S. Thesis.*